The Dissertation Committee for Lucas Richard Pettey Certifies that this is the approved version of the following dissertation:

Quantum Dynamics on Adaptive Grids: The Moving Boundary Truncation Method

Committee:

Robert E. Wyatt, Supervisor

Graeme Henkelman

Dmitrii E. Makarov

Kent F. Milfeld

Mary F. Wheeler

Quantum Dynamics on Adaptive Grids: The Moving Boundary Truncation Method

by

Lucas Richard Pettey, B.S.; M.S.

Dissertation

Presented to the Faculty of the Graduate School of

The University of Texas at Austin

in Partial Fulfillment

of the Requirements

for the Degree of

Doctor of Philosophy

The University of Texas at Austin

December 2008

Dedication

This dissertation is dedicated to my wife, Lynn Forney, for her unwavering support.

Acknowledgements

I would like to thank my parents, Karen and Frank Pettey, for instilling in me from the very beginning an intense curiosity and desire to learn. I would also like to thank Robert E. Wyatt for his endless supply of patience and guidance. In addition, I would like to thank Corey Trahan, Keith Hughes, and Sonya Garashchuk for their scientific discussions that contributed to this work.

Quantum Dynamics on Adaptive Grids: The Moving Boundary Truncation Method

Publication No._____

Lucas Richard Pettey, PhD.

The University of Texas at Austin, 2008

Supervisor: Robert Eugene Wyatt

A novel method for integrating the time-dependent Schrödinger equation is presented. The moving boundary truncation (MBT) method is a time-dependent adaptive method that can significantly reduce the number of grid points needed to perform accurate wave packet propagation while maintaining stability. Hydrodynamic quantum trajectories are used to adaptively define the boundaries and boundary conditions of a fixed grid. The result is a significant reduction in the number of grid points needed to perform accurate calculations. A variety of model potential energy surfaces are used to evaluate the method. Excellent agreement with fixed boundary grids was obtained for each example. By moving only the boundary points, stability was increased to the level of the full fixed grid.

Variations of the MBT method are developed which allow it to be applied to any potential energy surface and used with any propagation method. A variation of MBT is applied to the collinear $H+H_2$ reaction (using a LEPS potential) to demonstrate the stability and accuracy. Reaction probabilities are calculated for the three dimensional

non-rotating $O(^3P)+H_2$ and $O(^3P)+HD$ reactions to demonstrate that the MBT can be used with a variety of numerical propagation techniques.

Table of Contents

List of Figures

x

Chapter 1: Introduction

It is a central goal of science to understand the world and how it works on the deepest level possible. When there are observations in the world that cannot be explained by current scientific principles, new theories are developed. Any new theory must not only clarify and predict the unexplained observations, but it must also be reconciled with current scientific principles. In the early twentieth century, chemists and physicists faced observations that could not be explained with the principles of the time. Experimental observations of black body radiation and the photoelectric effect were impossible according to Newton's laws of physics. As a result, some of the most brilliant minds of the time developed quantum mechanics.

The principles of quantum mechanics were able to explain observations like black body radiation and the photoelectric effect. They can also be extended to describe "classical" motion so that they reconcile with Newton's laws of motion. Quantum mechanics hinges on the idea that matter can be described as both a particle and a wave. Heisenberg's uncertainty principle, a core component of quantum mechanics, dictates that we cannot measure both position and momentum with infinite precision. There is a finite amount of error in everything that we observe. For large objects, like humans, cars, golf balls, etc., this error is not significant and Newton's laws of motion can be used. For small objects, like atoms and subatomic particles, the Heisenberg uncertainty principle becomes important and the motion must be described by quantum mechanics. A new equation of motion was developed to explain the behavior of particles governed by quantum mechanics. The result is the Schrödinger equation, named for Erwin Schrödinger, the scientist who first purposed the idea, and in one dimension is:

$$i\hbar \frac{\partial \psi(x,t)}{\partial t} = \frac{-\hbar^2}{2m} \frac{\partial^2 \psi(x,t)}{\partial x^2} + V(x)\psi(x,t)$$

(1.1)

In this equation, $\psi(x,t)$ is a complex valued function called the wave function and gives a complete description of the system (or particle) of interest and $V(x)$ is the potential being applied to the system. The real valued quantity $\psi^*(x,t)\psi(x,t)$, often called the density of the wave function, is the probability of finding the particle at a given point, x, at a given time, t.

If the system is not varying in time, then the time independent version of the Schrödinger equation can be solved:

$$\frac{-\hbar^2}{2m}\frac{\partial^2\psi(x)}{\partial x^2} + V(x)\psi(x) = E\psi(x) \tag{1.2}$$

Here $\psi(x,t)$ is chosen to be an eigenfunction of the differential equation and E is an eigenvalue representing the total energy of the wave function. There are few real examples where there is an analytical solution to the time independent Schrödinger equation, but many times an approximation can be made to generate analytical solutions. Time independent solutions of the Schrödinger equation have been successfully applied to problems like atomic and molecular structure. These applications have given scientists a deeper understanding into why an atom or molecule might respond to an external potential, but in order to gain an understanding of how atoms react and develop rates of chemical reactions, the time dependent Schrödinger equation must be used.

Time-dependent solutions to the Schrödinger equation can provide great insights into chemical dynamics. Unfortunately, there are even less situations than in the time independent case where an analytical solution can be found. As such, approximations to the overall Schrödinger equations and numerical approximations must be used to solve the time dependent Schrödinger equation. Some approximations used in time dependent solutions of the Schrödinger equation will be discussed in Chapter 2. As for the numerical techniques used for propagating the solution to the time dependent Schrödinger equation, there are generally two competing concerns: accuracy and stability vs. efficiency. One way of obtaining accurate solutions is to evaluate the spatial

derivatives, either on a grid or through basis sets, and advance the solution in small time steps. There are a variety of well developed methods for obtaining the derivatives on large fixed grids, such as finite differences and finite element.

In a traditional fixed grid approach to numerical integration of the time-dependent Schrödinger equation, the wave function, as described above, is represented as the complex-valued function $\psi(x,t)$. The initial wave function is usually in the form of a wave packet. A wave packet is a superposition of standing waves, each with a different wavelength, weighted in such a way that the position and momentum are localized but still obey the Heisenberg uncertainty principle. The spatial and time domains are discretized such that $x = x_0...x_N (x_n = n\Delta x)$ and $t = t_0...t_K (t_k = k\Delta t)$. This function is then represented by values at grid points x_n, and time steps t_k: $\psi(x_n,t_k) = \Psi_n^k$. Initial value and boundary conditions for $\psi(x,t)$ are provided by equations:

$$\psi(x_n,t_0) = \Psi_n^0; \qquad \psi(x_0,t_0) = a; \qquad \psi(x_N,t_0) = b. \qquad (1.3)$$

One way of assigning boundary conditions is to set the boundary points far enough apart so the wave function can be calculated for all times of interest. This requires some advance knowledge of the movement and spreading of the wave packet. Another possibility is to set "absorbing potentials" at the boundaries [1-3]. This type of boundary condition forces $\psi(x,t)$ to decay smoothly to a small value at the boundary, but the total probability is not necessarily conserved. The spatial derivatives are then calculated numerically and the solution is advanced in small time steps.

The main drawback to the use of large fixed (Eulerian) grids is the number of calculations and amount of memory required to store data at all the grid points. This data may or may not be important at every time step. In quantum transport problems, for example, grid points introduced at early times where the wave packet initiates may not be needed at later times because the packet has moved to a different location. The result is wasted effort in calculating solutions for grid points that are of little significance to the overall dynamics of the problem.

One way to improve the efficiency of generating solutions is to use a trajectory method [4-9,12-24]. In trajectory methods, the wave function is discretized into small parts of probability that are propagated in time according quantum hydrodynamic equations of motion. The quantum hydrodynamic equations of motion for trajectory methods were developed by Bohm [10,11] as part of a program to develop an alternative to the traditional Copenhagen interpretation of quantum mechanics. These equations and their implications will be discussed in detail in Chapter 3. There are several methods to generate solutions based on trajectory dynamics, including the quantum trajectory method [5-7] (QTM) and the derivative propagation method [12,13] (DPM). These methods generally use significantly fewer points than fixed grid methods. There are several drawbacks to the hydrodynamic approach, including under or over sampling and preservation of accuracy near nodes in the density. There has recently been a great deal of work addressing these problems, including the use of a linearized quantum force [14-16], covering functions [17,18], arbitrary Lagrangian-Eulerian (ALE) grids [19-22], and hybrid methods [23,24].

All of the above methods will be discussed in detail in Chapter 3. In particular, the derivation of QTM and DPM will be presented. In addition to QTM and DPM, a thorough explanation of ALE and hybrid methods will be presented as they provided the inspiration for this work. In ALE, the boundaries of the grid are frequently moved at Lagrangian speeds, while the interior grid points move with a velocity that maintains constant spacing. This may be the perfect solution to the sampling problem, but moving grids have unique stability issues [25,26]. Various results of ALE calculations will be presented along with situations where ALE is unsuccessful in generating a solution. In hybrid methods a combination of trajectory methods and fixed Eulerian methods is implemented.

The unique approach developed in this study is to utilize quantum trajectories at the boundaries where the wave function is smooth and adapting a fixed grid in the

interior to compute the wave function by traditional fixed grid means. A full explanation of the initial form of the method [27,28] will be presented in Chapters 4 along with the results of model problems. The method uses the advantages of trajectory methods while avoiding some of the problems and inaccuracies that can develop by computing the bulk of the solution on a traditional fixed grid. The goal is to combine the accuracy of solving the Schrödinger equation on a fixed grid with the efficiency of trajectory methods. The interior grid points are stationary and the number involved at each time step varies based on the distance between the boundary trajectories. The result is a significant decrease in computational effort without loss of accuracy or stability. Chapter 5 introduces a generalized version of the method that has been proven on potential energy surfaces generated from *ab initio* calculations and with a variety of numerical propagators [29].

Chapter 2: The Born-Oppenheimer Approximation and Potential Energy Surfaces

2.1: THE BORN-OPPENHEIMER APPROXIMATION

In chemical dynamics, the complete Schrödinger equation is extremely difficult to solve. This is due to the large number of particles in a chemical system. The complete Hamiltonian (right hand side of the TDSE) for a chemical reaction is:

$$\hat{H} = \frac{-\hbar^2}{2m}\sum_{i=1}^{N}\nabla(\vec{r})_i^2 - \frac{\hbar^2}{2M_A}\sum_{A=1}^{M}\nabla(\vec{R})_A^2 - \sum_{i=1}^{N}\sum_{A=1}^{M}\frac{Z_A}{\vec{r}_{iA}} + \sum_{i=1}^{N}\sum_{j>i}^{N}\frac{1}{r_{ij}} + \sum_{A=1}^{M}\sum_{B>A}^{M}\frac{Z_A Z_B}{\vec{R}_{AB}} \qquad (2.1)$$

In this notation, lower case letters represent the N number of electrons in coordinate space $\vec{r}$ and capital letters represent the M number of nuclei in coordinate $\vec{R}$. A more compact form commonly used takes advantage of operator notation:

$$\hat{H} = \hat{T}_e(\vec{r}) + \hat{T}_N(\vec{R}) + \hat{V}_{Ne}(\vec{r},\vec{R}) + \hat{V}_e(\vec{r}) + \hat{V}_N(\vec{R}) \qquad (2.2)$$

Even for a molecule as simple as H_2, there is no known analytical solution to the Schrödinger equation. Two general approaches have been developed to generate approximate solutions to the TDSE for chemical systems. One approach involves creating efficient numerical methods for generating a solution to the TDSE and the bulk of this dissertation will describe a novel method developed for that purpose. A second approach is to simplify the Hamiltonian in some way in order to reduce the number of terms. A common application of the latter approach is called the Born-Oppenheimer approximation. The remainder of this chapter will describe this approximation and how it is used in chemical dynamics.

In examining Equation 2.2, there are two main groups of particles: electrons and nuclei. The mass of an electron is thousands of times smaller than the mass of a nucleus. As such, electrons are moving much faster than nuclei on average. The Born-Oppenheimer approximation states that this difference in motion allows the Schrödinger equation to be solved into two stages; one for the electrons and one for the nuclei. The

first stage involves solving a truncated version of the Hamiltonian which only concerns the electrons, often called the electronic Hamiltonian:

$$\hat{H} = \hat{T}_e(\vec{r}) + \hat{V}_{Ne}(\vec{r},\vec{R}) + \hat{V}_e(\vec{r})$$

(2.3)

It is important to note that this operator still has a dependence on the nuclear coordinate, $\vec{R}$. The nuclei are so slow in comparison to the electrons that they can be considered fixed and the electronic Hamiltonian becomes parametrically dependent on the nuclear coordinate:

$$\hat{H} = \hat{T}_e(\vec{r}) + \hat{V}_{Ne}(\vec{r};\vec{R}) + \hat{V}_e(\vec{r})$$

(2.4)

Eigenvalues and eigenstates for this operator can now be calculated at various fixed nuclear coordinates. If the nuclear portion of the Hamiltonian is also to be calculated, the eigenvalue obtained from the electronic Hamiltonian at given internuclear distance, $\vec{R}$, is added to the value of the nuclear potential operator, $\hat{V}_N(\vec{R})$. This process is then repeated for a variety of internuclear distances to generate a single potential energy surface only dependent on the nuclear coordinate, $V(\vec{R})$. This creates a second Hamiltonian for the nuclei, called the nuclear Hamiltonian,

$$\hat{H} = \hat{T}_N(\vec{R}) + V(\vec{R})$$

(2.5)

The Born-Oppenheimer approximation allows for quantum dynamics to be studied in chemical reactions. It holds well for situations where the electronic eigenstates are far apart in energy. As the eigenstates become closer in energy, some coupling must be considered. Large volumes of work exist and continue to be developed to incorporate this coupling in numerical calculations of chemical systems. In the remainder of this work, only the nuclear Hamiltonian will be considered (Eq. 2.5) and only potential energy surfaces dependent on a single eigenstate.

2.2 MODEL POTENTIAL ENERGY SURFACES

The simplest potential energy surface is derived from two nuclei involved in a chemical bond. The nuclei are attracted to each other so that the electrons can be shared,

and they also repel each other because both nuclei have positive charges. There is a distance, therefore, where the nuclei balance their attractive and repulsive forces. The nuclei are in constant motion, however, so the distance between them constantly oscillates around point of lowest energy called the equilibrium bond distance, R_e. The bond between the nuclei can be envisioned as a spring holding one nucleus to the other. If the bond gets stretched, the attractive forces pull the nuclei back together and if the nuclei get too close, their repulsive forces push them apart again. This model of the chemical bond is called the harmonic oscillator. The mathematical form of the potential energy surface is based on the displacement of a spring:

$$V(R) = \frac{1}{2}kR^2$$
(2.6).

The constant, k, is based on the attractive force between the nuclei. As vibrational energy increases, the maximum deflection from R_e also increases.

While the harmonic oscillator is a good model for nuclear vibration, at higher energy states the nuclei can achieve distances that are very far away or very close together. In reality, there is a distance beyond which the nuclei are no longer attracted to each other. At separations greater than this dissociation length, R_D, the electronic attraction is not strong enough to restore the chemical bond and the nuclei can move independently of each other. The simple harmonic oscillator does not account for this dissociation. The potential energy of the harmonic oscillator model also does not approach infinity quickly enough as the nuclei become close together. To correct these errors, a more complex type of vibrational model is often used called the Morse oscillator. The Morse oscillator has the form:

$$V(R) = hcD_e(1 - e^{a(R-R_e)})^2$$
(2.7)

where D_e is the depth of the potential surface and a is related to both k(force constant in the harmonic oscillator, Eq. 2.6) and D_e. The Morse oscillator accounts for dissociation as well as approaching infinity faster as the nuclei come close together. The Morse oscillator also has energy levels that become closer and closer together as dissociation is

approached. Both the harmonic oscillator and the Morse oscillator are simple ways of incorporating molecular vibration into a potential energy surface.

Modeling vibrations is important, but what about chemical reactions? Eckart in 1934 [30] first considered how to represent a simple chemical reaction in one dimension. He considered a three nuclei system following the reaction AB + C → A + BC. The nuclear potential for this system is represented in Figure 2.1.When atom C is far from molecule AB, the potential will resemble the vibration of molecule AB shown in Region 1 of Fig. 2.1. As atom C approaches, there will be a transition state ABC where all three nuclei are interacting (Region 2 in Fig. 2.1). Finally, as atom A moves away from molecule BC, the potential resembles the vibration of molecule BC seen in Region 3 of Figure 2.1. Eckart successfully reduced the potential energy surface to one dimension by moving along the minimum energy path. This is accomplished by finding the continuous line that connects all three regions while maintaining the lowest possible energy value. He derived an expression the shows how the potential energy varies moving from the equilibrium bond distance of the reactants, through the minimum transition state and into the equilibrium bond distance of the products. The resulting function is called the Eckart barrier and has the form:$V(x) = V_o \operatorname{sech}^2[a(x-x_b)]$, where V_o is the barrier height, a measures the barrier width, and x_b is the position of the barrier maximum. The symmetrical case in which products and reactants have the same energy is represented in Figure 2.2a. The barrier height represents the amount of energy the nuclei need to enter the transition state (Region 2 in Figure 2.1). Unsymmetrical cases are also possible in which the reactants and products have different energies. Extreme cases have the form: $V(x) = V_0 / (1 + e^{-a(x+x_b)})$ where the sign of V_o determines which side is higher in energy. A negative value for V_o generates a downhill ramp (Fig 2.2b) and could model exothermic reactions or photodissociation of an excited state. A positive V_o generates an uphill ramp (Fig 2.2c) representing an endothermic reaction or creation of an excited state. The slope of the ramp is determined by a and the midpoint is located at x_b. Linear
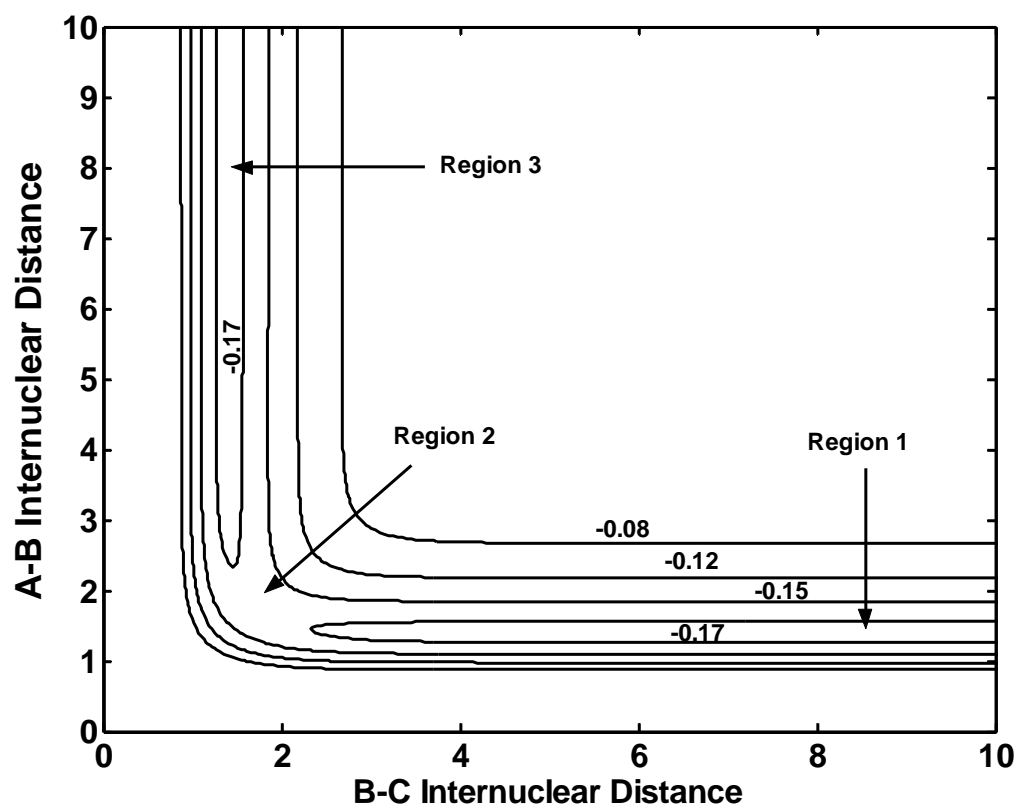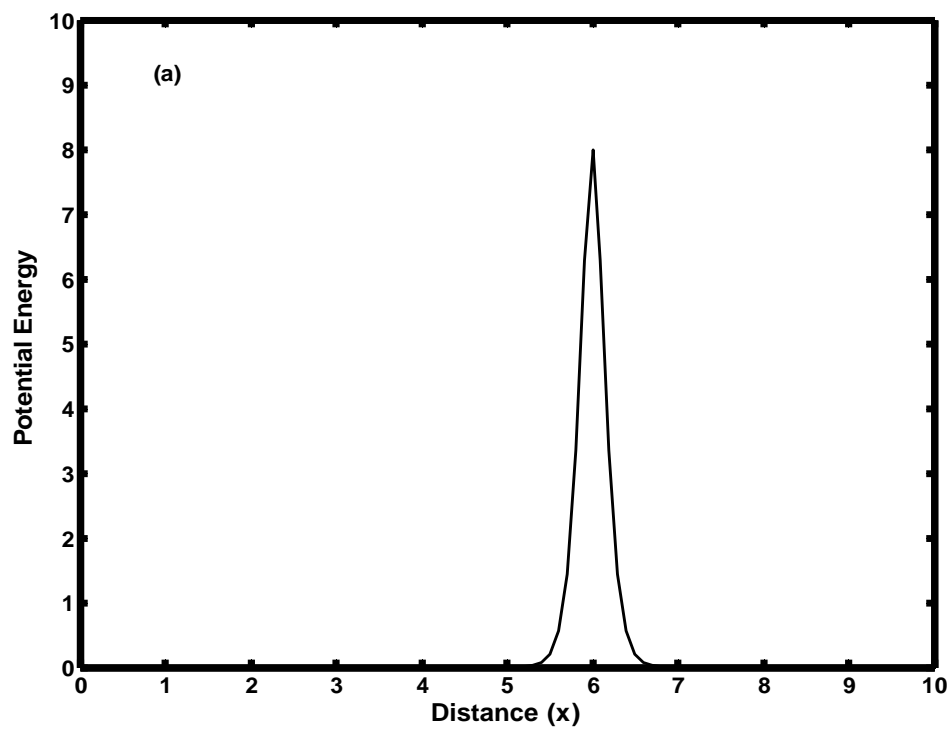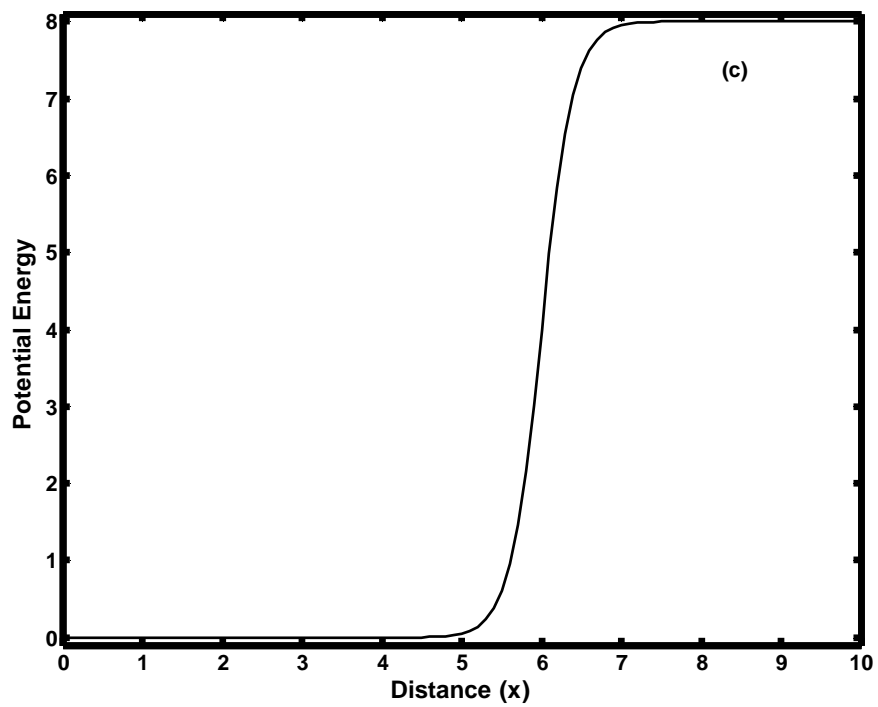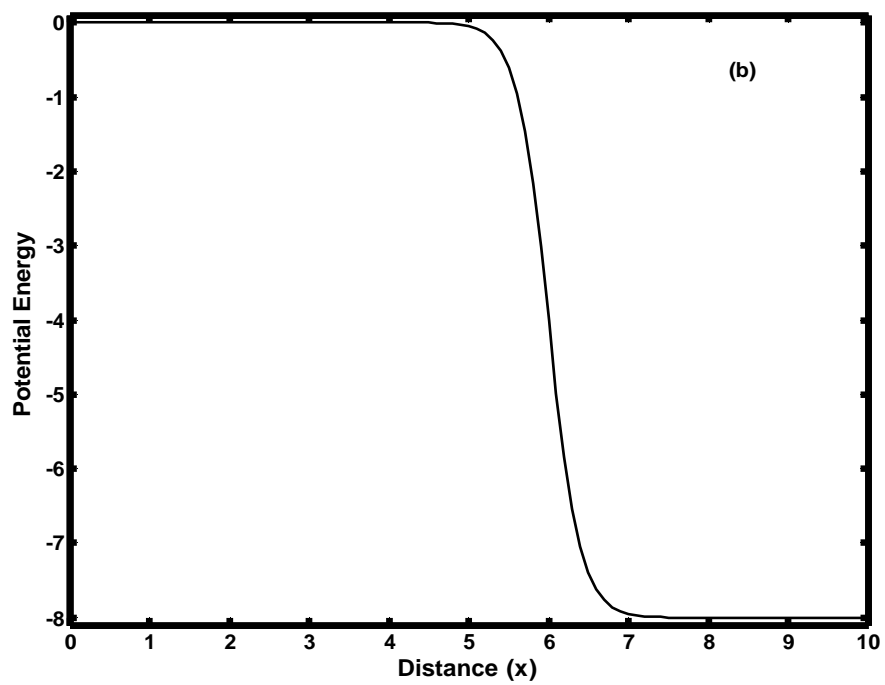
FIGURE 2.1 COLLINEAR REACTION BETWEEN AN ATOM AND A DIATOMIC MOLECULE.
Contours increase in energy from -0.17 to -0.08 *a.u.*

FIGURE 2.2 VARIOUS ONE DIMENSIONAL MODEL POTENTIAL ENERGY SURFACES WITH THE SAME PARAMETERS, $V_0 = 8; x_b = 6; a = 5$. a) The symmetric Eckart barrier. b) The downhill ramp. c) The uphill ramp.

combinations of the symmetrical barrier and the uphill ramp can represent an endothermic reaction that has an activation barrier whereas a combination of the symmetric barrier and the downhill ramp will represent an exothermic reaction.

Potential energy surfaces utilizing harmonic oscillators, Morse oscillators, and Eckart barriers are often called "model" potential energy surfaces since they are not directly related to a specific chemical system. The parameters of the model can be carefully chosen to approximate a chemical system and thus new methods, like the one presented in this work, are usually first demonstrated on a model surface.

2.3 REALISTIC POTENTIAL ENERGY SURFACES

More robust potential energy surfaces are necessary in order to calculate dynamics for specific chemical reactions. One of the most popular energy surfaces is representative of the $H+H_2$ chemical reaction. In addition to the models presented earlier, it is also a very common test for a new numerical method. The surface used in this work was developed by Sato [31]. It is based on earlier works by London, Eyring and Polanyi so it is often abbreviated as a LEPS potential energy surface. The surface is based on the idea that that the minimum energy for a three atom system occurs in the collinear state. Examination of this surface in Figure 2.3 shows why the model potentials are frequently used in developing new methods. The LEPS surface is qualitatively similar to an Eckart barrier coupled to a Morse oscillator. The main difference is that the LEPS surface is "bent", i.e. the barrier region is the apex of an angle between the reactant and product regions. An additional term can often be added when coupling a Morse oscillator to an Eckart barrier to simulate this bending. There are more complex differences between the two potential energy surfaces, however. The most significant difference is that the analytical form of the LEPS surface is much more complicated than the Eckart barrier coupled to a Morse oscillator. This makes analytical differentiation of the LEPS surface difficult. Numerical derivatives can be calculated, but their accuracy will be dependent on the grid spacing which can affect the stability of a numerical method.
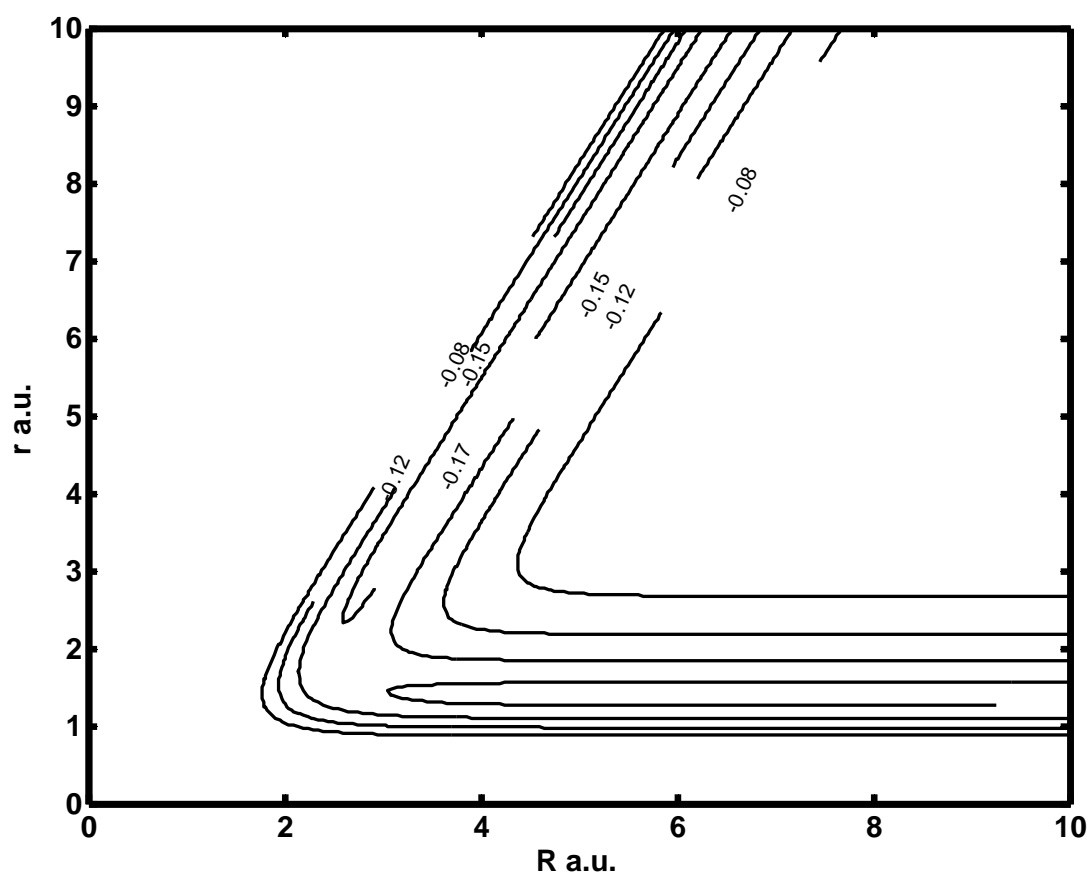
FIGURE 2.3 THE LEPS COLLINEAR H+H$_2$ REACTION POTENTIAL ENERGY SURFACE.
Potential energy contours range form -0.17 *a.u.* to -0.08*a.u.*.

The most sophisticated type of potential energy surface is generated using *ab initio* quantum mechanical calculations. Surfaces of this type are created by solving the electronic Hamiltonian for a variety of nuclear geometries and then fitting the resulting energies to some type of analytical form based on the nuclear coordinate. The accuracy of the surface is determined by the number of geometries involved in the fitting and the type of calculation used to obtain the electronic energies. The number of nuclear geometries used is generally the minimum necessary to achieve a low rms error in the fitting. Usually, additional geometries not involved in the fitting procedure are then calculated and compared to the fitted surface to insure accuracy. There are a variety of ways for calculating the electronic energy values, but all involve some combination of atomic orbitals. By using a greater number of atomic orbitals, the accuracy of the electronic energies increases. Whenever possible, barrier heights from surfaces are compared to experimental activation energies as an additional method for evaluating the accuracy of the potential energy surface.

The specific potential energy surface used in this work is based on the $O(^3P)$ $+H_2(v = 0; j = 0) \rightarrow OH + H$ reaction in the $^3A^{'}$ state originally developed by Rogers, et. al. [32]. The potential surface was developed by first calculating the energy of 951 different geometries using a complete-active-space-self-consistent-field (CASSCF) internally contracted configuration interaction (ICCI) method. Of the 951 geometires, 112 were selected for "high accuracy" calculations that involved a greater number of orbitals in the basis set. The energy of these geometries was then fitted to a surface using the generalized London-Eyring-Polanyi-Sato double polynomial (GLDP) method [32]. This method creates a surface which is extremely accurate. The rms error is only 0.0117 eV with a maximum error of 0.0169 eV. The error is calculated by comparing CASSCF-ICCI calculations to GLDP values for geometries not included in the original fitting. Another measure of error was the comparison of several features in the surface to experimental data. Unfortunately, this specific reaction is very difficult to isolate

experimentally, so no barrier height comparisons could be made. Comparisons could be made between the dissociation energy of H_2 and OH calculated by the surface and those values generated by experiment. This analysis showed that the fitted surface was within 0.2 kcal/mole or 0.008eV.

The surface that is generated by the procedure described above is shown in Figure 2.4, plotted in cylindrical coordinates. In this coordinate system, R is the distance between the O atom and the H_2 diatomic; r is the distance between the two H atoms and θ is the angle between R and r. It contains three channels; one reactant $O+H_2$, and two product channels OH+H. The product region of the potential surface is defined as the region where the OH bond length is less then 3.5 a_0 and transmission probability is the integration $P_{trans} = \int\int\int \psi^*\psi \sin\theta \, d\theta \, dR \, dr$ over this region. There are two minimum energy paths (MEPs) corresponding to the two collinear configurations ($\theta=0$ and $\theta=\pi$) shown in Figures 2.4c and 2.4d. Moving along these MEPs, the maximum barrier height is 0.565 eV . The overall reaction is slightly endothermic, as the product channel of the MEPs is 0.11eV higher in energy than the reactant channel. The top down views in Figure 2.4(b,d) appear similar to the 2D LEPS surface shown earlier. There are some additional contours in the product region, but these can only be accessed by going over a second barrier or through the original barrier region but from a different rotational angle. The importance of this additional path to the product channel will be demonstrated later.

FIGURE 2.4. ISOSURFACES OF THE O(^{3}P) $+$H$_2$($v = 0$; $j = 0$) $\rightarrow$ OH $+$H $^3A'$ POTENTIAL
ENERGY SURFACE. (a) Reactant and product channels of the 0.5 eV potential
surface. (b) Top view of (a) showing that the channels are not connected at
this energy level. (c) Isosurfaces of the 0.5 eV (blue) and 0.75 eV (red)
potential energy surfaces. At the angles near $\theta = 0$ and $\theta = \pi$, the reactant
and product channels are connected showing the barrier. (d) Top down view
of (c).

(c)

(d)
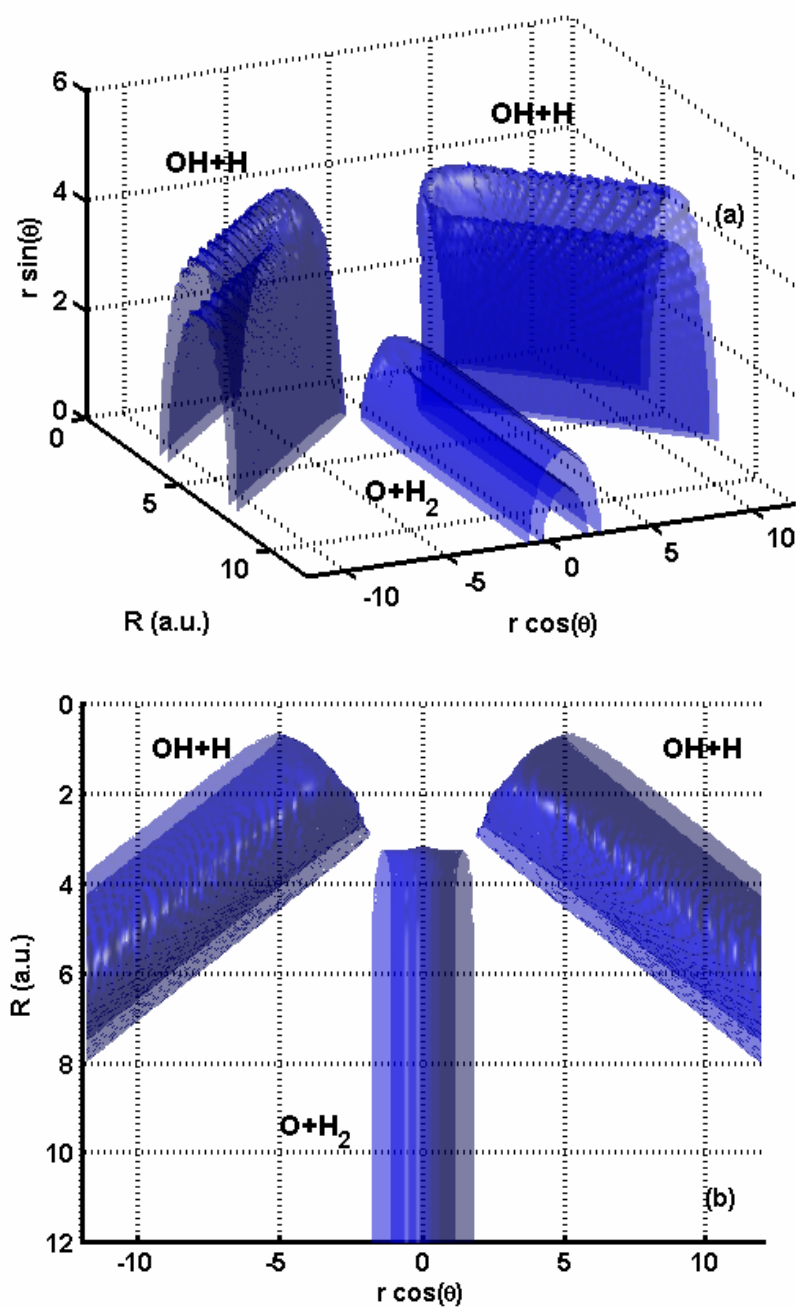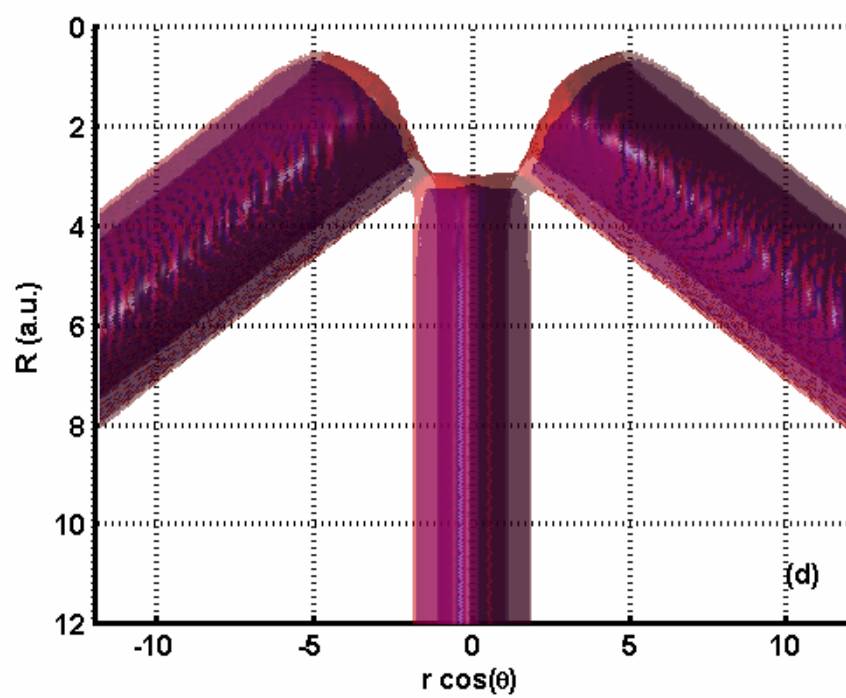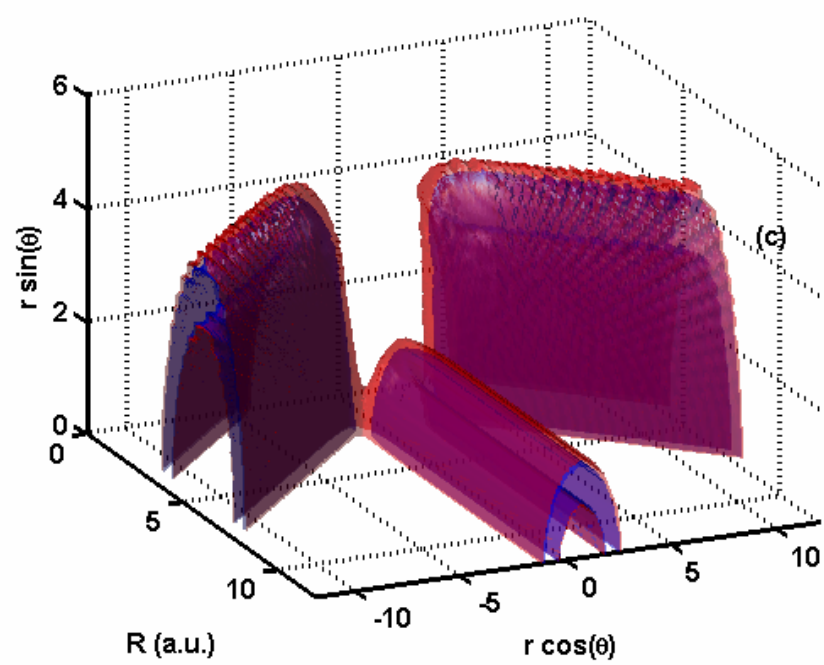
Chapter 3: Quantum Hydrodynamic Equations of Motion

3.1 BOHMIAN MECHANICS

The most popular interpretation of quantum mechanics comes from the Copenhagen doctrine. In this interpretation, the wave function contains all possible information about a system. Operators are applied to the wave function in order to determine the probability of observing a particular physical quantity. The wave function, the Schrödinger equation, and all operators are purely statistical in nature. They do not describe physical processes of particles in a system; they simply describe the probability of measuring a particular physical quantity of the system.

While this interpretation is mathematically sound and can produce useful information, many scientists over the years, including Einstein, yearned for a deterministic approach to quantum mechanics. There are a variety of interpretations of quantum mechanics in the world of physics that attempt to produce the same results as the statistical Copenhagen approach while still connecting to physical processes. One such approach was first considered by de Broglie and further developed by Bohm [10,11]. It is referred to as the deBroglie-Bohm interpretation of quantum mechanics or simply Bohmian mechanics.

In Bohmian mechanics, a casual interpretation of the Schrödinger equation is made so that more commonly understood principles such as force can be described. The fundamental difference between Bohmian mechanics and the Copenhagen interpretation is the importance of particles on the system. In Bohmian mechanics, the system exists as a collection of particles whose motion can be describe by a wave whereas in the Copenhagen interpretation the wave function is the complete description of the system. The mathematical form of the wave is the complex valued function $\psi(\bar{r},t)$ and $\psi(\bar{r},t)$ must be a solution to the Schrödinger equation. The particles move according to the gradient of the phase of the wave function. This guidance condition classifies

Bohmian mechanics as a pilot wave theory. The fact that the particles are introduced also makes Bohmian mechanics a "hidden variable" theory. In fact, the particles are the hidden variables!

A common misconception about Bohmian mechanics is that it violates the Heisenberg uncertainty principle. The Heisenberg uncertainty principle states that both the position and momentum of a particle can only be known within a finite precision. Bohmian mechanics appears to violate this principle because individual particles with known positions are following trajectories based on the guidance condition with known velocities. While individual trajectories do exist, the uncertainty principle is conserved because the starting position is unknown. In Bohmian mechanics, as in classical mechanics, an ensemble of particles is evolved, each according to its individual guidance condition. The initial ensemble of particles has a distribution of $\psi^*(\vec{r},0)\psi(\vec{r},0)$. Since $\psi(\vec{r},t)$ is a solution to the Schrödinger equation, the initial distribution of particles obeys the uncertainty principle and the propagation of the ensemble also follows the uncertainty principle.

Bohmian mechanics can be described mathematically by using the polar form of the wave function $\psi(\vec{r},t) = R(\vec{r},t)e^{iS(\vec{r},t)/\hbar}$, where R and S are real functions representing the amplitude and phase. Inserting this polar form into the TDSE and separating the real and imaginary parts yields the quantum hydrodynamic equations of motion (QHEM):

$$i\hbar\frac{\partial}{\partial t}\left[R(\vec{r},t)e^{iS(\vec{r},t)/\hbar}\right] = -\frac{\hbar^2}{2m}\nabla^2\left[R(\vec{r},t)e^{iS(\vec{r},t)/\hbar}\right] + V(\vec{r},t)\left[R(\vec{r},t)e^{iS(\vec{r},t)/\hbar}\right]$$

$$\text{(imaginary part)} \quad \frac{\partial R(\vec{r},t)}{\partial t} = -\frac{1}{m}\nabla R(\vec{r},t)\nabla S(\vec{r},t) - \frac{1}{2m}R(\vec{r},t)\nabla^2 S(\vec{r},t)$$

$$\text{(real part)} \quad -\frac{\partial S(\vec{r},t)}{\partial t} = -\frac{\hbar^2}{2m}\frac{1}{R(\vec{r},t)}\nabla^2 R(\vec{r},t) + \frac{1}{2m}\left(\nabla S(\vec{r},t)\right)^2 + V(\vec{r},t)$$

$$(3.1)$$

The quantity, $-\frac{\hbar^2}{2m}\frac{1}{R(\vec{r},t)}\nabla^2 R(\vec{r},t)$, is often called the quantum potential, Q, because it is the only term that explicitly involves $\hbar$ and is the source of all quantum effects. If the partial time derivatives in Equation 3.1 are replaced with total time derivatives

$(\dfrac{df}{dt} = \dfrac{\partial f}{\partial t} + \dfrac{d\vec{r}}{dt}\nabla f$) by taking the viewpoint of moving along the trajectory with its velocity, $\dfrac{d\vec{r}}{dt} = \dfrac{1}{m}\nabla S(\vec{r},t)$, known as the Lagrangian frame, then the equations become:

$$\frac{dR(\vec{r},t)}{dt} = -\frac{1}{2m}R(\vec{r},t)\nabla^2 S(\vec{r},t)$$

$$\frac{dS(\vec{r},t)}{dt} = \frac{1}{2m}(\nabla S(\vec{r},t))^2 - (V(\vec{r},t)+Q(\vec{r},t))$$

(3.2)

The first equation in Equation 3.2 is the continuity equation. It is similar to the continuity equation from fluid dynamics. This equation insures that probability is conserved by the wave function. The second equation is the Quantum Hamilton-Jacobi equation. It is very similar to the Hamilton-Jacobi equation except that it contains the quantum potential. One can see from this equation that the quantum potential is aptly named for two reasons. First, it has units of energy like a standard potential. Second, if the gradient operator is applied, then after manipulation a dispersion force term arises. If this term is absent, the dynamics of the wave function are completely the same as in classical mechanics.

These two equations show how Bohmian mechanics can be considered attractive from an interpretation standpoint. The equations can be directly related to classical mechanics. The additional quantum potential term "converts" a system into quantum mechanics. If $\hbar$ approaches zero or mass approaches infinity, popularly termed the "classical limit", the quantum potential vanishes and classical mechanics are recovered. While the Copenhagen interpretation can yield the classical limit, the derivation is quite lengthy. Second, the continuity equation allows probability to be viewed as a fluid moving through the classical potential surfaces while constantly being dispersed by the quantum potential.

3.2 THE QUANTUM TRAJECTORY METHOD

Although Bohmian mechanics generates equations which may be more attractive from an interpretation standpoint, numerical solutions can be more difficult to obtain. The

two main reasons are that instead of one equation, there are two and the equations are also nonlinear. There have been many attempts recently to perform calculations on physical systems using Bohmian mechanics. The first major numerical approach was developed by Wyatt and co-workers called the quantum trajectory method (QTM) [5-7]. This approach sought to take advantage of the classical analogs in Bohmian mechanics. The basic premise is to launch an ensemble of trajectories that follow paths dictated by quantum mechanics using the QHEM formulated earlier. These trajectories are pieces of the probability distribution and the ensemble carries all of the information about the system. At any point, the wave function can be reconstructed from the trajectories and operators can be applied as in the Copenhagen interpretation.

The first step in QTM is to recast the QHEM into the Lagrangian frame as shown in Equation 3.2. Next, an initial ensemble of trajectories is chosen. Each trajectory carries a certain amount of probability with it according to the size of its volume element and the initial distribution of the wave function $\psi^*(\bar{r},0)\psi(\bar{r},0)$. The trajectories are propagated in a series of time steps. At each time step, the velocity of a trajectory is updated as well as the amplitude and phase of the wave function carried by that trajectory. The trajectories do need to be evenly spaced initially, and even if they are, they usually form an unstructured grid very quickly. In order to calculate the necessary derivatives for updating the velocity, amplitude and phase along a trajectory, QTM uses a moving weighted least squares (MWLS) method. The MWLS method works in a similar fashion to other numerical methods for calculating derivatives. First a stencil is drawn around the trajectory being calculated. The size of the stencil is set either so that all trajectories within a fixed distance are included in the fitting, or a fixed number of trajectories closest to the trajectory of interest are used. Once the stencil is set, the amplitude and phase are locally fit to a basis set. Generally, polynomials are used as a basis set, but other basis functions, such as a radial basis set [33], have been successfully used. After fitting, local

derivatives are calculated so that velocity, amplitude and phase can all be updated. The process is repeated at each time step for every trajectory in the ensemble.

The QTM propagation scheme has been very successful in calculating transmission probabilities for a variety of barrier scattering problems and in many degrees of freedom. There are some drawbacks that can occur while using QTM, however. The first involves spacing of the trajectories. By allowing each trajectory to move at its Lagrangian velocity, the ensemble may spread in such a way that certain areas of the potential become under sampled. The wave function is only known at points where trajectories exist, so if the trajectories spread, the wave function will not be known in between the trajectories. If the trajectories spread too far, the MWLS can become unstable. In a similar fashion, if the trajectories coalesce towards a common location, compression occurs. In compression, there are too many trajectories in a given element of space. Numerical errors can develop and the propagation can break down.

The second drawback in the QTM procedure is inherent to Bohmian mechanics. Examining the quantum potential, one can see that the phase of the wave function propagates in time proportionally to the inverse of the amplitude. As the amplitude approaches zero, the quantum potential becomes infinite. This is known as the "node problem" since it occurs at nodes in the wave function where density has gone to or is approaching zero. Fortunately, quantum trajectories never enter nodes. They do, however, accelerate rapidly as they approach and ultimately avoid a node. This rapid change in velocity can cause instability in the MWLS fitting procedure. It also inherently results in an undersampling condition in areas around the node. Nodes can be of particular interest since they represent areas of interference. Resolving nodes is a continuing challenge in the numerical implementation of Bohmian mechanics.

There are a variety of methods for dealing with the propagation difficulties presented quantum trajectories such approximate quantum forces [14-16], covering functions [17,18], the derivative propagation method (DPM) [12,13], aribitrary

Lagrangian-Eulerian (ALE) grids [19-22], and hybrid methods [23,24]. A detailed description of approximate quantum force methods and covering functions along with detailed results can be found in the literature. In brief, approximate quantum force methods change the quantum potential so that it is no longer related to the exact amplitude. Rather, it is fit either to a linear or exponential basis set. This prevents nodes from causing numerical inaccuracies, but also makes the method generate approximate solutions rather than exact calculations of quantum dynamics. In covering functions, the superposition principle is exploited to stabilize the numerically solutions to the QHEM. The superposition principle states that wave functions which satisfy the constraints of the Schrödinger equation can be added and subtracted from each other to form new wave functions that also are acceptable to the Schrödinger equation. When implementing a covering function method, a new wave function is added to the wave function of interest in order to cover up the nodes and create a new total wave function for propagation, i.e. the areas of nodes in the wave function are now non zero and thus the quantum potential is not infinite. The original wave function can always be recalculated by subtracting the known covering function. This has been successfully applied to barrier scattering, but a careful choice must be in determining the covering function and it may not necessarily stabilize the gradient of the amplitude and phase near a node. The last three methods of the list (DPM, ALE and hybrid methods) were the impetus for the novel method presented in this work. Each will be considered in detail below.

3.3 THE DERIVATIVE PROPAGATION METHOD

In the derivative propagation method, trajectories are propagated independently of the rest of the ensemble. This is accomplished by carrying all the necessary information along the trajectory path. In the DPM, analytical equations of motion are derived for the spatial derivatives, thus trajectories can be propagated with only the information carried by them. The higher order derivatives carry the necessary non-local information to preserve quantum effects such as tunneling. The equations are derived by applying the

spatial derivative operator to Eqs. 3.2 and then changing the order of differentiation on the left-hand side:

$$\nabla \frac{dR(\vec{r},t)}{dt} = \nabla\left[-\frac{1}{2m}R(\vec{r},t)\nabla^2 S(\vec{r},t)\right]$$

$$\nabla \frac{dS(\vec{r},t)}{dt} = \nabla\left[\frac{1}{2m}(\nabla S(\vec{r},t))^2 - (V(\vec{r},t)+Q(\vec{r},t))\right]$$

$$\frac{d\nabla R(\vec{r},t)}{dt} = \nabla\left[-\frac{1}{2m}R(\vec{r},t)\nabla^2 S(\vec{r},t)\right]$$

$$\frac{d\nabla S(\vec{r},t)}{dt} = \nabla\left[\frac{1}{2m}(\nabla S(\vec{r},t))^2 - (V(\vec{r},t)+Q(\vec{r},t))\right]$$

(3.3)

The result is an infinite hierarchy of equations for both the functions and their derivatives. The hierarchy can be terminated when the solution can be approximated by a low-order polynomial, since all spatial derivatives of higher order than the polynomial will be zero. When DPM is used with the QHEM, the amplitude of the wave function $R(\vec{r},t)$ is represented by $e^{C(\vec{r},t)}$, where $C(\vec{r},t)$ is a low order polynomial. This substitution allows the hierarchy of derivatives to be truncated at a reasonably low order, usually between second and fourth. DPM has been successfully applied to a variety of barrier scattering problems, other equations of motion in phase space such as the Wigner and Klein Kramers equations and a relatively new approach based on representing the QHEM in the complex plane.

DPM is not a perfect solution to the node problem, however, as the method has some unique issues that arise during a calculation. The trajectories can still spread and compress creating areas of over and under sampling. This can be circumvented by altering the velocities of the trajectories, but adjusting trajectory velocity in order to fully sample a region eliminates the advantage of propagating the trajectories independently. Perhaps a more serious disadvantage is that the low order polynomial approximation is not always valid, particularly near nodes. Also, as will be shown later in this work, trajectories may not be stable on potential energy surfaces that do not have analytical derivatives.

3.4 ARBITRARY LANGRANGIAN-EULERIAN METHODS

The arbitrary Langrangian-Eulerian (ALE) methods are based on the idea that the velocity of a trajectory does not need to be the Lagrangian velocity. Although the Lagrangian velocity is the "natural" velocity at which a trajectory will move in response to the forces acting on it, any velocity can be used. In ALE, trajectories define the boundary of a grid and move at their Lagrangian velocities. This insures that the grid will capture the entire wave packet. Each interior grid point has a unique velocity at each time step that must be factored into the QHEM:

$$\frac{\partial R(\vec{r},t)}{\partial t} = -\frac{1}{m}\nabla R(\vec{r},t)\nabla S(\vec{r},t) - \frac{1}{2m}R(\vec{r},t)\nabla^2 S(\vec{r},t) + \left(\frac{d}{dt}\vec{r}\right)\nabla R(\vec{r},t)$$

$$-\frac{\partial S(\vec{r},t)}{\partial t} = -\frac{\hbar^2}{2m}\frac{1}{R(\vec{r},t)}\nabla^2 R(\vec{r},t) + \frac{1}{2m}\left(\nabla S(\vec{r},t)\right)^2 + V(\vec{r},t) + \left(\frac{d}{dt}\vec{r}\right)\nabla S(\vec{r},t)$$

. (3.4)

When Trahan and Wyatt [22] implemented ALE, they used a series of "smart springs" in between the grid points in order to maintain proper spacing but allow for capturing the dynamics of the system. The springs were based on a monitor function, $M(\vec{r},t)$, and the grid points were set such that the monitor function was equally distributed among them: $\int_i^{i+1} M(\vec{r},t)dr = \text{constant}$. The velocity of each grid point was determined by how far it had to move in order to maintain this equidistribution of the monitor function. The monitor function was chosen based on the curvature of the amplitude. In addition, a minimum grid spacing was enforced so that grid points never became so close as to become unstable.

This technique was successful under conditions which caused traditional QTM methods to fail. The monitor function coupled with the minimum grid spacing insured that compression of grid points did not cause numerical errors while also ensuring that the regions of interference in the wave function were properly sampled. The method did not address the inherent instabilities of nodal regions caused by the QHEM. It also required additional computational effort to maintain the equidistribution of the monitor function and maintain its minimum grid spacing.

A different implementation of ALE was developed by Kendrick [19-21]. In this approach, the interior grid points maintain a constant spacing. Grid points are added or deleted as necessary in order to maintain this constant spacing. There are several advantages of this form of ALE. First, by maintaining fixed grid spacing between the interior grid points, any numerical method can be used to determine the derivatives of the amplitude and phase. Second, under sampling and over sampling will never occur because the grid points are forced to remain a fixed distance from each other. One disadvantage of ALE is that since the grid points are no longer moving at their Lagrangian velocities, they may move into the vicinity of a node in the amplitude. When this happens, the derivatives can be very difficult to accurately evaluate numerically. Kendrick dealt with these instabilities by introducing an "artificial viscosity" to stabilize the velocity equations. The artificial viscosity acts like a potential and is based on the curvature of the local velocity. Since the velocity of a trajectory will increase near a node, this helps to alleviate the numerical instabilities. Kendrick [21] successfully applied this method to a variety of scattering potentials in multiple dimensions. The generalized method, while successful, requires a significant amount of computational cost to calculate the artificial viscosity and re-grid when adding or deleting grid points.

3.5 HYBRID METHODS

Other attempts at resolving the problems with numerical implementation of Bohmian mechanics involve mixing the polar form of the wave function and the associated QHEM with more traditional methods of solving the Schrödinger equation. These "hybrid methods" blend the two interpretations of quantum mechanics and numerical techniques for solving the Schrödinger equation in order to create a single method that has the advantages of both interpretations. The motivation is based on the idea that moving grids can be more efficient in calculations while techniques based on the traditional form of the Schrödinger equation are more stable in regions of interference where nodes can form.

The first attempt at a hybrid method was developed by Hughes and Wyatt [23]. They took the ALE approach developed earlier by Trahan and Wyatt and adapted it to a traditional, non-Bohmian viewpoint. It was not a full moving grid because the end points were held fixed. It was an adaptive grid technique based on the moving path transform of the Schrödinger equation. The end points of the grid were held fixed and the equidistribution principle was used to distribute the grid points as in the earlier ALE approach. The monitor function used was based on the curvature of the wave function.

This hybrid method was successfully applied to an Eckart barrier scattering calculation and a double well. One of the disadvantages of the method was the use of an interpolation grid. A Chebyshev pseudospectrals propagation technique was used for the kinetic energy operator. This technique requires that the grid points correspond to nodes in the polynomials. Since the grid points were moving according to the equidistribution principle, a second set of grid points located at the Chebyshev nodes are necessary. Interpolation was performed between the two grids to generate the overall solution and propagate it in time. A smoothing function was used in addition to the monitor function to determine grid point velocity. This was necessary to prevent oscillations in the paths of the grid points that would cause instabilities.

A second hybrid method was developed by Babyuk and Wyatt [24]. In this method, the propagation of the wave packet on a scattering potential was divided into stages. The initial stage consisted of the wave packet approaching the barrier. The QHEM using QTM advanced the calculation in time. The second stage began when the wave packet neared the barrier and parts of it began to reflect. At this point, a combination of traditional methods on a fixed grid and QHEM on an ALE grid was used to continue the calculation. The fixed grid, traditional methods were utilized on the reflected side of the barrier where as the QHEM-ALE approach was used to calculate the transmitted portion of the wave packet. The third stage involved separating the transmitted and reflected wave packets and propagating them independently. Since the third stage did not begin

until all nodes vanished, the QHEM on an ALE grid could be used to propagate the independent pieces of the wave packet.

The method was extremely successful for calculating the scattering of a wave packet on an Eckart barrier. The main disadvantage to this approach is the stages of the propagation must be clearly identified. Even after identifying the stages of propagation, the various grids and representations of the wave function must be reconciled. This requires overlap of the two grids during the second stage. Also, during the second stage an absorbing potential is required to eliminate artificial oscillations in the wave function. In the third stage, the leading edge of the reflected packet required a constant velocity rather than its Lagrangian velocity for stability and grid points on the leading edge were eliminated when their density became lower than a threshold value. Using these constraints, the calculation was stable for over 1 ns of propagation.

3.5 A NEW ALE-HYBRID METHOD

Another type of hybrid ALE method not yet presented in the literature was tested before the new technique described in this work was developed. In this formulation, quantum trajectories were used at the boundaries and the interior grid points moved with velocities that insured spacing was equal, similar to the approach of Kendrick. The main difference is that the interior points are not propagated using the QHEM. They are propagated using the moving path transform as presented by Hughes and Wyatt [23]:

$$i\hbar \frac{d\psi(\vec{r},t)}{dt} = \left[-\frac{\hbar^2}{2m}\nabla^2 + V(\vec{r}) + i\hbar\dot{\vec{r}} \cdot \nabla \right]\psi(\vec{r},t)$$

$$\tag{3.5}$$

In order to propagate the quantum trajectories without the overlap problems encountered in the approach of Babyuk and Wyatt, DPM is used for the trajectories at the end points. DPM allows the trajectories at the boundaries to be moved independently since all of the necessary information is carried along with the trajectory. Since the interior grid points retain uniform spacing, any traditional method of calculating derivatives can be used for propagation without interpolation.

The first test of this new approach was wave packet scattering against an Eckart barrier. The calculation was stable and efficient. The results were extremely accurate compared to a fixed Eulerian calculation. Unfortunately, this method is not applicable to all potential energy surfaces. In fact, the simple uphill and downhill ramp calculations cannot be performed with this hybrid ALE approach. The reason for the failure may lie in the advective term added to the to the Schrödinger equation in its moving path transform. In order for a moving grid to be stable, it is important for the grid velocity to closely match the natural velocity at that point. If it does not, this advective term can become unstable and cause the solution to fail. In both the uphill and downhill ramps, the area of the ramp has a dispersive velocity. In the downhill ramp, a classical trajectory would move along the ramp. In the uphill ramp, the trajectory would move along the ramp until it either got to the top and continued forward or ran out of energy and then moved backwards. Quantum trajectories would not act much differently, although some of the downhill ramp quantum trajectories would also reflect backwards. In the ALE calculation, however, both edges of the gird are expanding. In order to maintain fixed grid spacing, the points in the middle have a very low velocity. This means that the points are moving much slower and possibly in the wrong direction compared to their Lagrangian velocities. The difference in grid velocity and Lagrangian velocity is probably the main reason this approach was unsuccessful for these simple potentials, as various time steps and grid spacings were attempted to eliminate propagation errors without any success.

The fact that this ALE approach was unsuccessful on simple potentials is unfortunate, but it raises an important question. If the advective term can become unstable when the grid point velocity is not close to the Lagrangian velocity, how can fixed grid spacing be used while maintaining the advantages of a moving grid? The answer is to not move the interior grid points at all. The remainder of this work will be dedicated to describing how a fixed, Eulerian grid can be used to propagate a wave

packet while maintaining the advantages of a moving grid by letting quantum trajectories guide the boundaries of the grid.

Chapter 4: The Moving Boundary Truncation Method using the Derivative Propagation Method

4.1 ONE DIMENSIONAL FORMULATION

We begin with a wave function $\psi(x,t)$ and discretize it as in Eq. (1.3). The boundaries are set to capture the significant portions of the initial density and represent the locations from which the quantum trajectories will be launched. In practice, $\psi(x,0)$ is decaying towards zero at the boundaries, so the trajectories are usually launched from points where the density has decayed to <0.0001. This grid will have the structure shown in Fig. 4.1(a). The spatial derivatives are calculated for the solid dots, and the open circles represent grid points where $\psi(x,t)$ is set to zero. Although $\psi(x,t)$ is set to zero at these points, they may be included in the calculation of the derivatives at non-zero points, for example, in center differences. However, only the nonzero parts of $\psi(x,t)$ (at the solid points) are advanced in time. Quantum trajectories are launched from the boundaries represented by the asterisks in Fig. 4.1(a). They are moved according to their Lagrangian velocity $\dot{x} = 1/m(\partial S(x,t)/\partial x)$ and their dynamics are governed by Eqs. (3.3). The trajectories do not need to coincide with the fixed grid points; however that is usually a convenient starting point. If the boundary trajectories move a distance larger than Δx, the grid adapts so that new fixed grid points are defined, $x_{-1} = x_0 - \Delta x$ or $x_{N+1} = x_N + \Delta x$, as necessary. This is demonstrated in Fig. 4.1(b). The value of $\psi(x,t)$ at the new grid point is interpolated from the value of the boundary trajectory as it passes the newly acquired fixed grid point. Now the grid is defined for t_1 and values are in place to advance the solution from t_1 to t_2. The process is repeated at each time step until the final solution is reached.
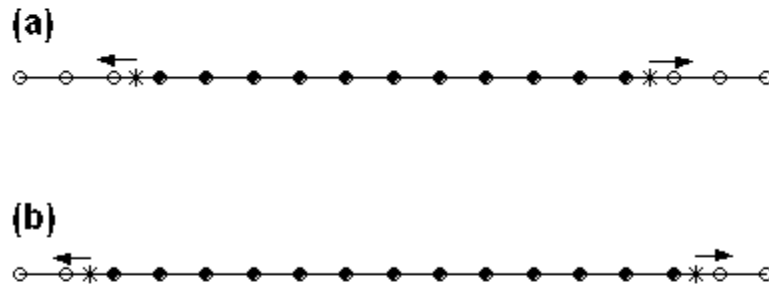
(a)

(b)

FIGURE 4.1 GRID POINT ACTIVATION BY TRAJECTORIES. a) Initial set of fixed grid points selected to represent the wave function are shown as filled circles. Open circles are grid points not included in the dynamics at this time step. Trajectories (asterisks) are launched from the boundaries in the direction of the arrows. b) After the boundary trajectories move past fixed grid points, they pass function and derivative information to the new fixed grid points to be included in the dynamics.

If the solution fractures into segments separated by large x regions where $\psi(x,t)$ is very small, the internal grid can also be split and multiple boundary trajectories would then exist. The grid will adapt to the significant portions of $\psi(x,t)$ *without any advance knowledge of the dynamics*. Once the boundaries have highlighted the fixed grid points relevant to the wave packet at a given time step, the solution is propagated on the fixed grid.

Wave packet dynamics on three different one dimensional model potentials were the first calculations made to evaluate the method described above. Scattering from an Eckart barrier was examined to determine how well the method calculated transmission probabilities and preserved both the oscillatory structure and the nodes in the wave function. The barrier is the same as used by Lopreore and Wyatt in their first quantum trajectory studies [5]. The other two potentials were the uphill and downhill ramps. They were chosen because of the breakdown of fixed grid ALE approaches.

The first example involves scattering from the Eckart potential: $V(x) = V_o \sec h^2[a(x - x_b)]$, where V_o is the barrier height, a measures the barrier width, and x_b is the position of the barrier maximum. The parameters for this study are 8000 cm^{-1}, 0.5 *a.u.*, and 6 *a.u.*, respectively. The initial condition is a Gaussian wave packet centered at the origin: $\psi(x,0) = (2\beta/\pi)^{1/4} \exp(-\beta x^2 + ikx)$, where β=10 *a.u.* and the initial energy is $E = \hbar^2 k^2 / 2m$. A range of initial energies were used, from 10 to 12000 cm^{-1}. Both a full fixed grid and a moving boundary truncated grid were compared using the same grid spacing (0.05*a.u.*). The boundary trajectories were moved according to their Lagrangian velocity. Figure 4.2 shows the energy dependence of the transmission probability at 75 fs, calculated by integrating the wavefunction for all $x \geq 6$ at each time step. The truncated grid (markers) generates nearly identical results as the full grid (solid line), with less than 1% difference in transmission probability between the two methods. The advantage of the truncated grid is shown in Figure 4.3. Part (a) shows the probability

density for the wave packet with initial energy of 8000 cm^{-1} at time zero. The truncated grid only requires 36 points to represent the initial density, but the full fixed grid required 1012 grid points since it must account for future changes in the density. Part (b) shows the density at 37.5 fs. The truncated and full grid results are in excellent agreement, but the truncated grid has adapted to cover the significant portions of the density by growing to 504 points. At 75 fs, shown in Fig. 3(c), the truncated grid has grown to match the full grid and correctly identifies the necessary grid points to capture more than 99.99% of the density. The average time needed for the truncated grid calculations was 12.23 s while the full grid required nearly twice as long, with an average of 24.01 s on an Athlon 2.19GHz processor with 1.00 GB of RAM.

The next example concerns wave packet scattering on an uphill ramp. This potential has the form $V(x) = V_o / (1 + e^{-a(x+x_b)})$ as described in Chapter 2. The uphill ramp studies utilized a potential with parameters V_o=1500 cm^{-1}, a=2.5 *a.u.*, and x_b=1 *a.u.* Initial wave packets with energies of 500, 1500, 3000, 4500, and 6000 cm^{-1} and centered at the origin were studied. These packets all showed bifurcation even if the initial energy was larger than that of the ramp. Figure 4.5 shows convergence of the transmission probability for various initial energies. The truncated and full grid results are in agreement within 0.2% at 100 fs. Figure 4.4(a) shows the initial density for a wave packet with an energy of 3000 cm^{-1}. The initial truncated grid contains 31 points and the grid expands to 952 points at 100 fs of propagation, as shown in Fig. 4.4(c). The full fixed grid utilized 952 grid points for all time steps and required an average of 19.44 s to perform the calculation. The truncated grid required an average time of 11.60 s, finishing 40% faster. In the truncated grid results, small oscillations occur that are not present in the full fixed grid. They can be seen in Fig. 4.4(b), which shows the wave packet at 50 fs and also in Fig. 4.4(c). These oscillations are present after approximately 5 fs of propagation, but they do not affect the qualitative shape of the wave packet or the
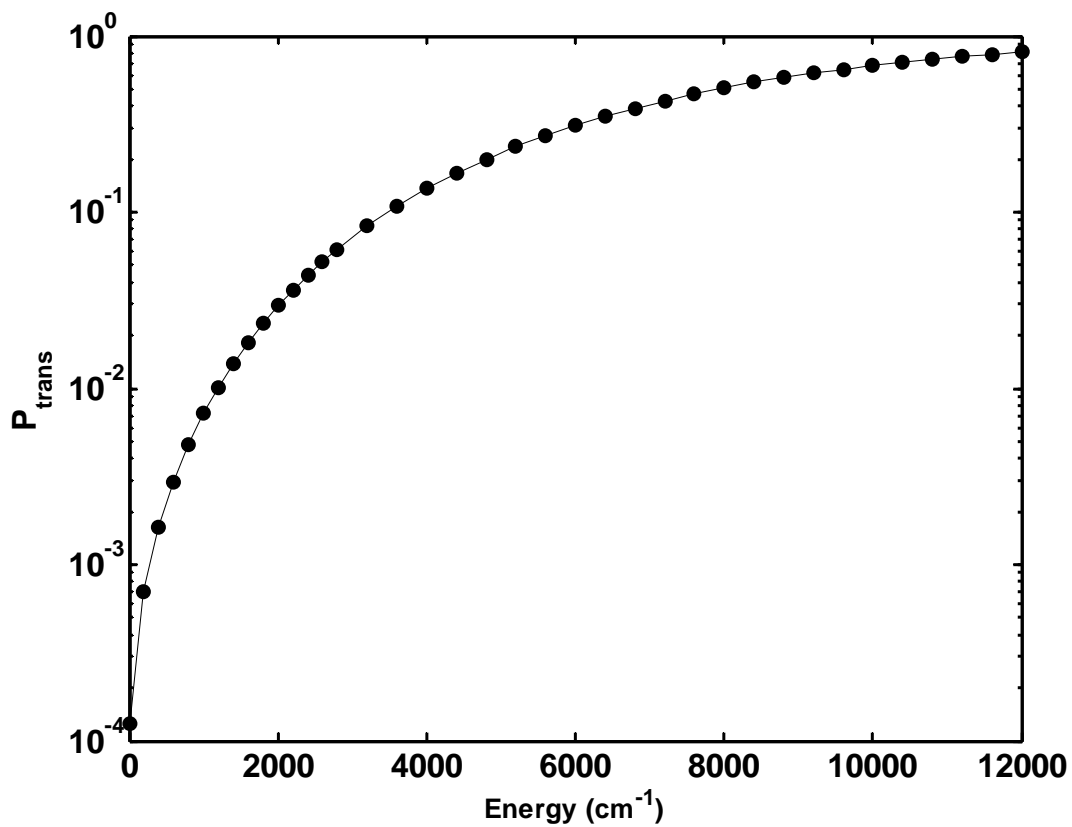
FIGURE 4.2 CONVERGED TRANSMISSION PROBABILITY AS AFUNCTION OF INITIAL KINETIC ENERGY FOR A WAVE PACKET SCATTERING OFF OF AN ECKART BARRIER. The solid line displays the full grid results while the markers indicate the results of the MBT calculations.
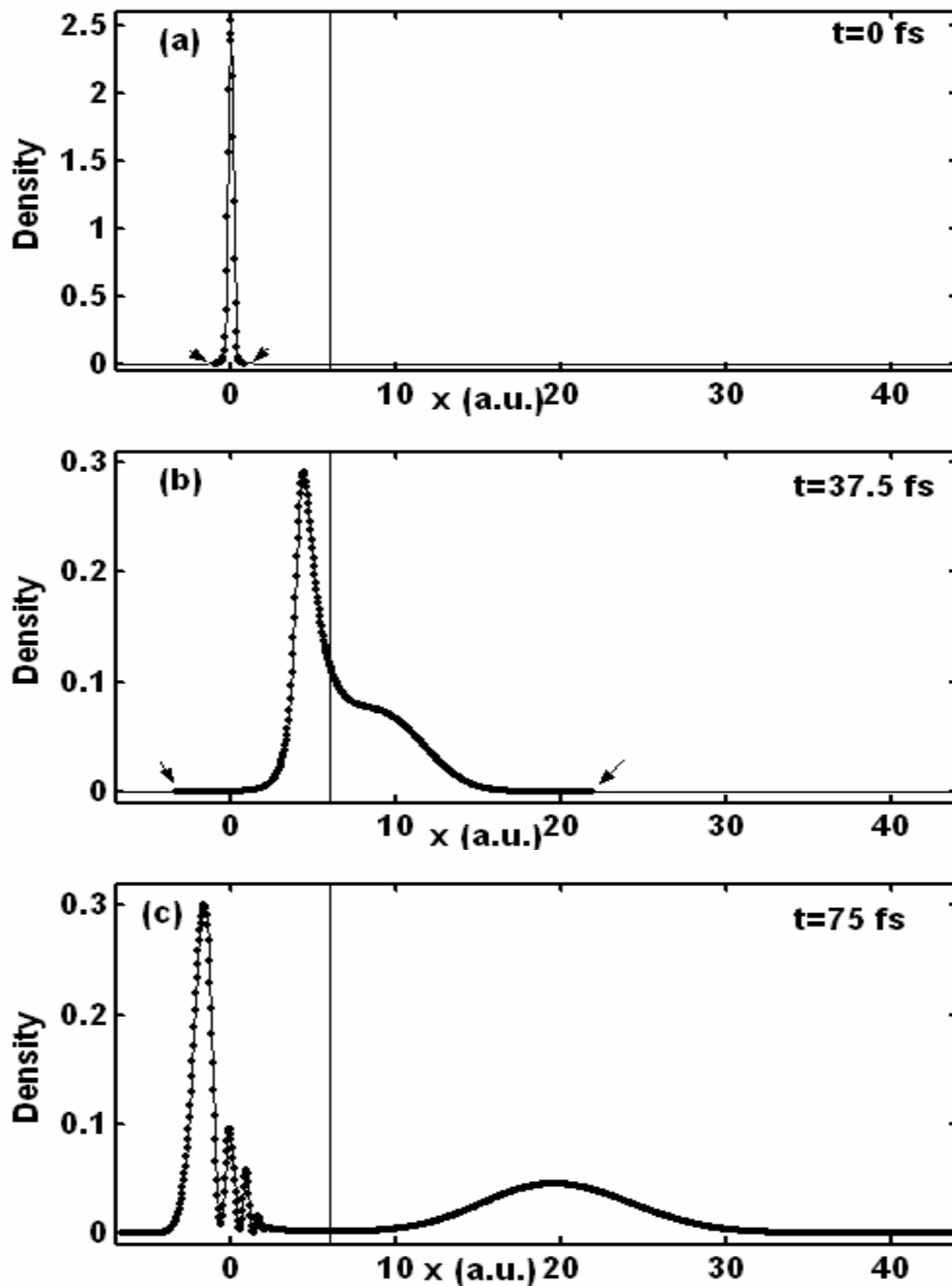
FIGURE 4.3: SCATTERING OF A WAVE PACKET WITH INITIAL WAVE PACKET WITH 8000 CM^{-1} ENERGY ON AN ECKART BARRIER. Points represent the truncated grid and the solid line represents the full grid a). Initially, the truncated grid used only 36 points and the boundaries are indicated with arrows. The vertical line at $x = 6$ marks the position of the barrier maximum. b) Wave packet at 37.5 fs. The truncated grid has expanded to 504 points but still uses fewer points than the full grid. c) Wave packet at 75 fs. The truncated grid has expanded the same number of points (1012) as the full grid.

stability of the calculation. Transmission probabilities are also largely unaffected, although minor oscillations can be seen in Fig. 4.5 in the plateau regions of the curves.

The downhill ramp potential that was studied had the same features as the uphill ramp except that the barrier height was negative, e.g. V_o =-1500 cm^{-1}, a =2.5 $a.u.$, and x_b =1 $a.u.$ The initial energies of the wave packets were 0, 375, 750, 1125, and 1500 cm^{-1}. In classical dynamics, the density would simply roll down the hill. In a quantum setting, the wave packet bifurcates, even though perfect transmission might be expected. This is not the case as can be seen in the exploded view of the transmission probabilities in Figure 4.6a. The low energy wave packets have a converged transmission probability less than one. A small portion stays above the hill. Also, a portion of the zero energy wave packet actually rolls down the hill although in classical mechanics the packet should remain stationary atop the barrier. Excellent agreement with the full grid results were obtained, just as for the uphill ramp studies. Pictures of the wave packet are not presented because these fragments that remain atop of the barrier are visually undetectable.

4.2 MULTIDIMENSIONAL MOVING BOUNDARY GRID TRUNCATION

The extension to multidimensional grids is straightforward in theory, but can have complications in practice. If the trajectories are moved at their Lagrangian speeds, they will very quickly become unstructured and some method must be devised to determine which fixed grid points are significant at a given time step. Another option is to restrict the trajectories to move in a single degree of freedom. Unfortunately, the trajectories are no longer moving in a purely Lagrangian fashion and thus can cross. This may cause problems near regions of interference where these approximate quantum trajectories may cross and prematurely truncate the fixed grid. A third option is to take the minimum and maximum trajectory positions in each degree of freedom as the boundaries of the fixed grid. This may mean that extra grid points which are outside the trajectories are included in the MBT calculation. Each of these methods has its advantages and disadvantages. The
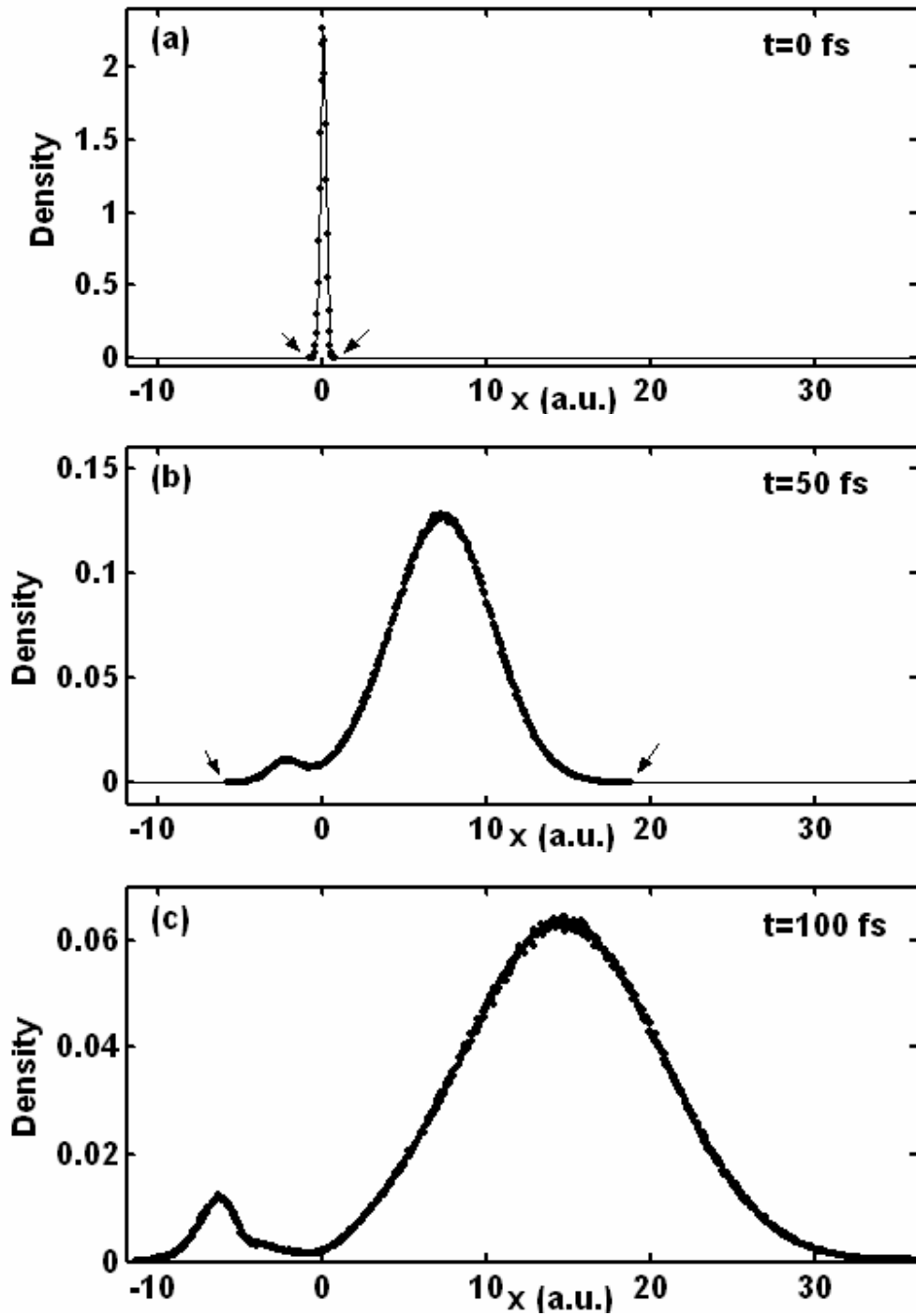
FIGURE 4.4: A WAVE PACKET WITH 3000 CM^{-1} ENERGY ON THE UPHILL RAMP POTENTIAL
a) Initial packet. The truncated grid used only 31 points and the boundaries
are indicated with arrows. b) Wave packet at 50 fs. The truncated grid has
expanded to 491 points, while the full grid uses 953. Some deviation of the
truncated grid results (points) can be observed relative to those on the full grid
(solid line). c) Wave packet at 100 fs. The truncated grid has expanded to the
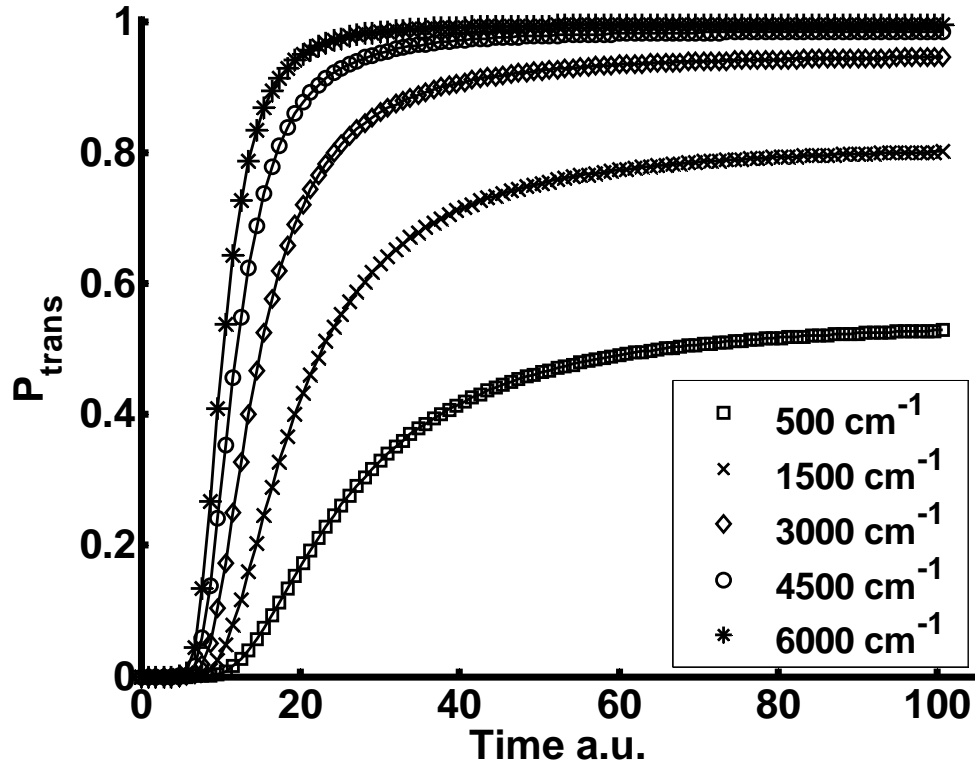same number of points as the full grid.

FIGURE 4.5: TRANSMISSION PROBABILITIES OF WAVE PACKETS WITH VARIOUS INITIAL KINETIC ENERGIES SCATTERING OFF OF THE UPHILL RAMP. Makers are calculated by the MBT method, while the solid lines are calculated using a full fixed Eulerian grid.
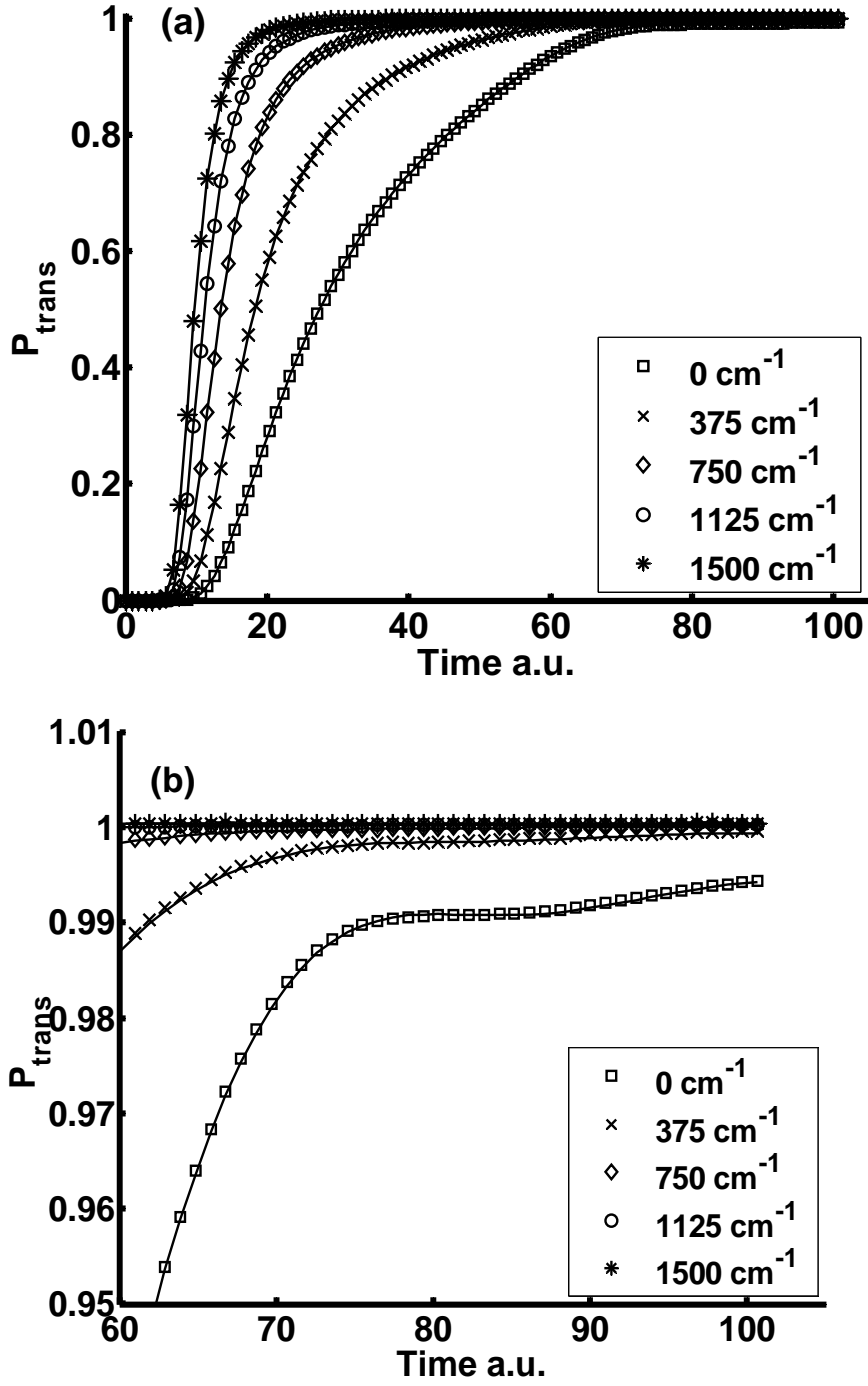
FIGURE 4.6: TRANSMISSION PROBABILITIES OF WAVE PACKETS WITH VARIOUS INITIAL KINETIC ENERGIES SCATTERING OFF OF THE DOWNHILL RAMP. Makers are calculated by the MBT method, while the solid lines are calculated using a full fixed Eulerian grid. a) Full scale transmission probabilities. b) Exploded view of the converged transmission probabilities showing the low energy packets do not completely converge to 1.

multidimensional examples presented below utilize various combinations of the three options in order to create the most efficient calculation.

The potential surfaces for the multidimensional examples are based on the reaction path Hamiltonian for collinear collisions of the type A + BC. The surfaces are obtained by transforming from Jacobi coordinates to natural collision coordinates $\{s, q_1, q_2, \ldots q_n\}$. In these coordinates, the surface is more linear with s representing the distance along the reaction path and q_n is a vibrational degree of freedom perpendicular to the reaction path. For the 2D system the potential is of the form: $V(s,q) = V_0 \sec h^2(as) + \frac{1}{2} k(s)q^2$. The s-dependent force constant for the vibrational degree of freedom introduces coupling in the form of $k(s) = k_0\left[1 - \sigma \exp(-\lambda s^2)\right]$. The potential parameters are similar to those used by Wyatt [7], Kendrick [20], and Trahan, et. al. [13], namely $V_0 = 8000cm^{-1}$, $a = .4a_0^{-1}$, $k_0 = 0.1909 a.u.$, $\sigma = 0.15$, and $\lambda = 0.25 a_0^{-2}$. The initial wave function is the product of the ground state for the vibrational degree of freedom and a Gaussian wave packet in the reaction path coordinate. This wavefunction is then multiplied by a plane wave in the positive s direction and has the general form:

$$\psi(s,q) = \left(\frac{4\beta_s\beta_q}{\pi^2}\right)^{1/2} \exp[-\beta_s(s-s_0)^2 - \beta_q(q-q_0)^2 + iks]$$

The initial widths of the Gaussian wavepackets are $\beta_s = \beta_q = 8 a.u.$. The reduced mass is 1837.152 and the initial wave packet energy, $E = \left(\hbar^2 k^2\right)/(2\mu)$, varied from 500 to 12000 cm^{-1}. In both the 2D and 3D cases, the trajectories are placed at points where the density of the initial wave packet has decayed to 0.0001. The trajectories are propagated using a fourth order DPM scheme.

The 2-D MBT results are in excellent agreement with the full fixed grid. The transmission probability as shown in Fig. 4.6(a) was calculated as $\int_0^\infty \int_{-\infty}^\infty \psi^*\psi dq ds$ at 46 f.s.. The error in transmission probability is 0.7-2.3%. The MBT calculations took on average 70% of the time that the full fixed grid required. Figure 4.7 shows how the MBT gains

this time advantage in a contour plot of the density at various times for the case where the initial energy was 10,000 cm^{-1}. Figure 4.7(a) shows the initial density and only 378 grid points are used for the wave packet on the truncated grid whereas the full grid used 11,394 points. 24 trajectories were used to guide the boundary conditions; however fewer might have been possible. After 22.7 f.s. of propagation, the truncated grid has grown to 3740 points as shown in Fig. 4.7(b). The trajectories have correctly spread to incorporate 99.99% of the density on the truncated grid. By the time transmission probability has converged at 45.4 f.s. in Fig 4.7(c), the truncated grid has expanded to 11,394 points, the size of the full grid. Small variations in the contours for the full grid and the truncated grid can be observed in Figs. 4.7(b) and 4.7(c). These differences appear to be similar to the oscillations seen in the one-dimensional study. Just as seen earlier, the minor variations do not significantly affect the qualitative shape of the wave packet or the transmission probability. Further propagation results in the trajectories continuing to expand. The boundary trajectories will never form two elliptical shapes representing transmitted and reflected packets. In order to form two independent elliptical shapes rather than one large spread ellipse, trajectories from the interior of the initial wave packet would need to be launched. These could then form the trailing edge of the transmitted and reflected packets.

In the 3D example, a second harmonic oscillator is coupled to the reaction path identical to the one already present in the 2D potential. The vibrational degrees of freedom are not coupled to one another, they are only coupled to the reaction path and they have the same force constant. The initial 3D wavepacket is the 2D wave packet multiplied by the ground state of the second oscillator with initial conditions $\beta_s = \beta_{q1} = \beta_{q2} = 8 a.u.$. Seventy trajectories were used to define the boundaries of the initial truncated grid at points where the initial density had decayed to <0.0001.

Once again, the MBT performs extremely well compared to the full fixed grid as shown in Figure 4.6b. The error in transmission probability was 0.13-4.7%. The MBT

was more efficient than the full fixed grid, finishing on average in 47% of the time required for the full grid. For the wave packet with an initial energy of 10,000 cm-1 as shown in Fig 4.9(a), the truncated grid started with 11,132 points compared to 427,194 points of the full fixed grid. After 29 fs, the truncated grid has expanded to 105,600 points and by the time transmission probability has converged at 58 fs, the truncated grid has grown to the size of the full grid. The isosurfaces in Figs. 4.9(b) and 4.9(c) show that the truncated grid maintains the correct shape of the wavefunction as well as converging to the correct transmission probability. Even under extremely close examination, it is difficult to pick out differences between the truncated grid and full grid isosurfaces.
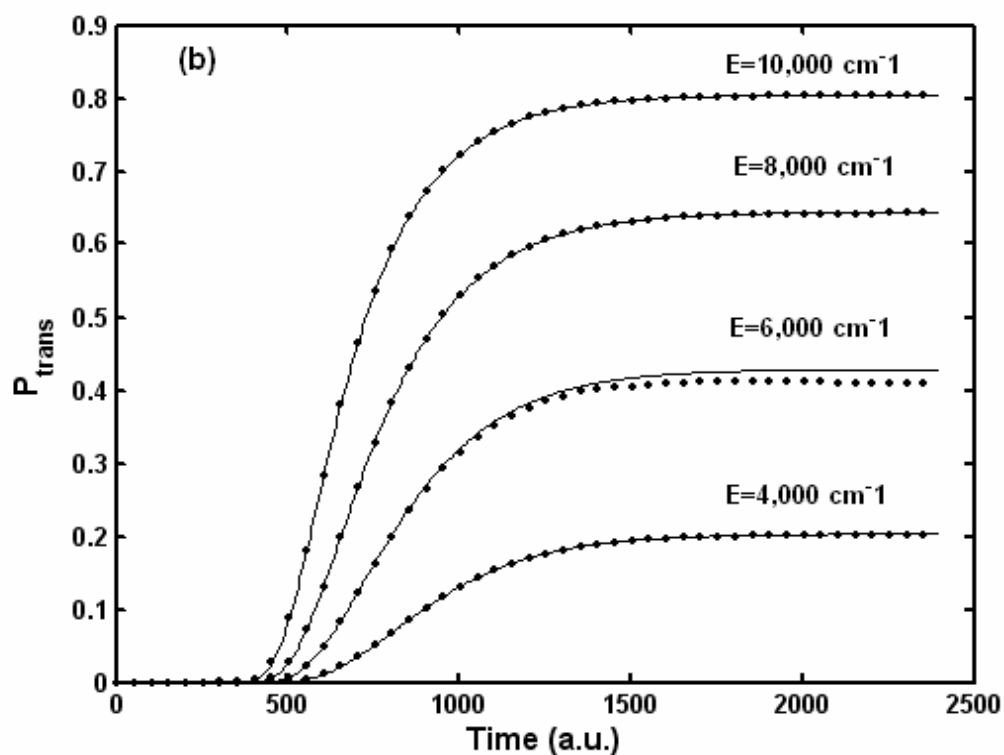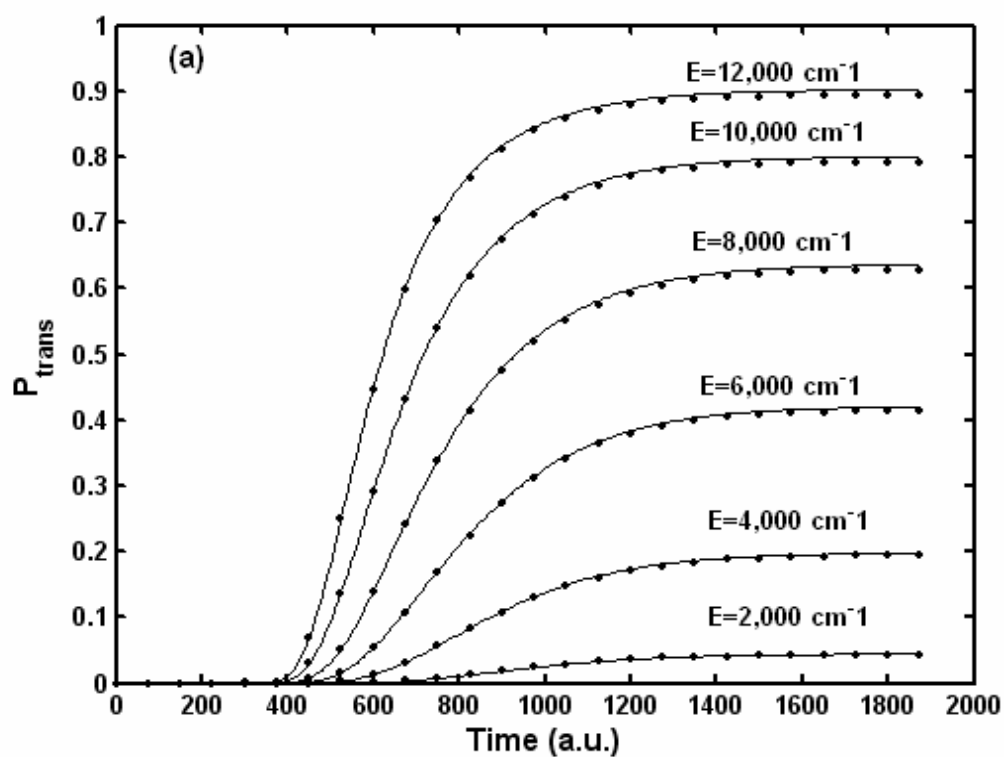
FIGURE 4.6 TRANSMISSION PROBABILITIES FOR MULTIDIMENSIONAL WAVE PACKETS. a) An Eckart barrier coupled to one harmonic oscillator. b) An Eckart barrier coupled to two harmonic oscillators.
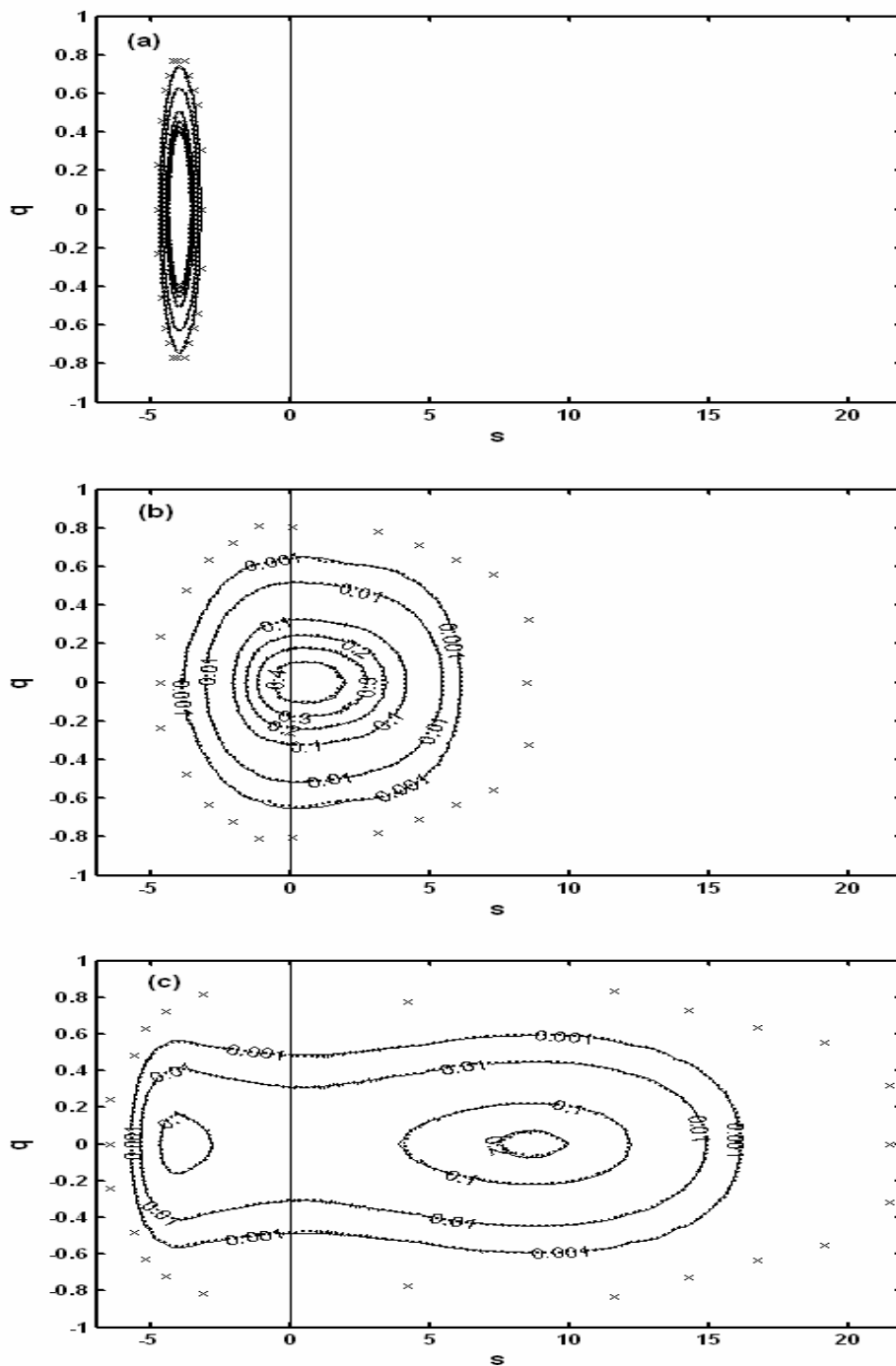
FIGURE 4.7: CONTOUR PLOTS OF THE WAVEPACKET WITH 10000 CM^{-1} INITIAL ENERGY IN THE TWO-DIMENSIONAL STUDY AT VARIOUS TIMES. The dotted contours represent the truncated grid results, while the solid contours correspond to the full grid. The trajectories that define the truncated grid are indicated by markers and the vertical line at $s = 0$ represents the position of the barrier maximum. a) Initial wave packet. b) Wave packet at 22.7 fs. The truncated grid has expanded as shown by the new positions of the trajectories, but still uses fewer points than the full grid. c) Wave packet at 45.4 fs. The truncated grid has expanded the same number of points as the full grid.

-46-

FIGURE 4.9: ISOSURFACES OF THE WAVEPACKET WITH 10000 CM^{-1} INITIAL ENERGY IN THE THREE-DIMENSIONAL STUDY AT VARIOUS TIMES. The isosurfaces are at densities of .001, .1, and .3 for the full grid. The wireframe surface is the truncated grid at a density of .001. The plane at $s = 0$ represents the position of the barrier maximum. a) Initial wave packet. b) Wave packet at 29 fs. The truncated grid has expanded, but still uses fewer points than the full grid. c) Wave packet at 58 fs. The truncated grid has expanded the same number of points as the full grid.
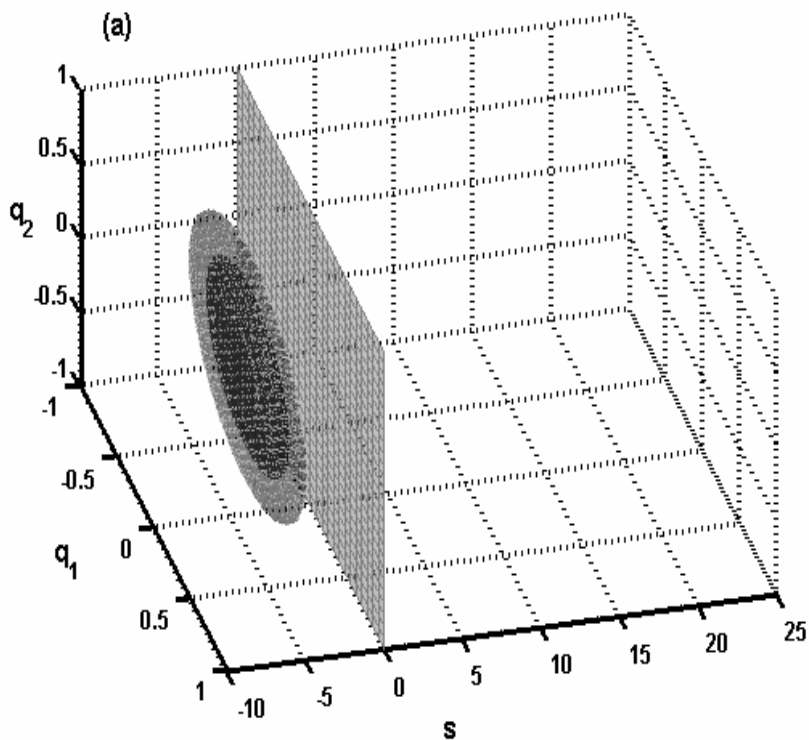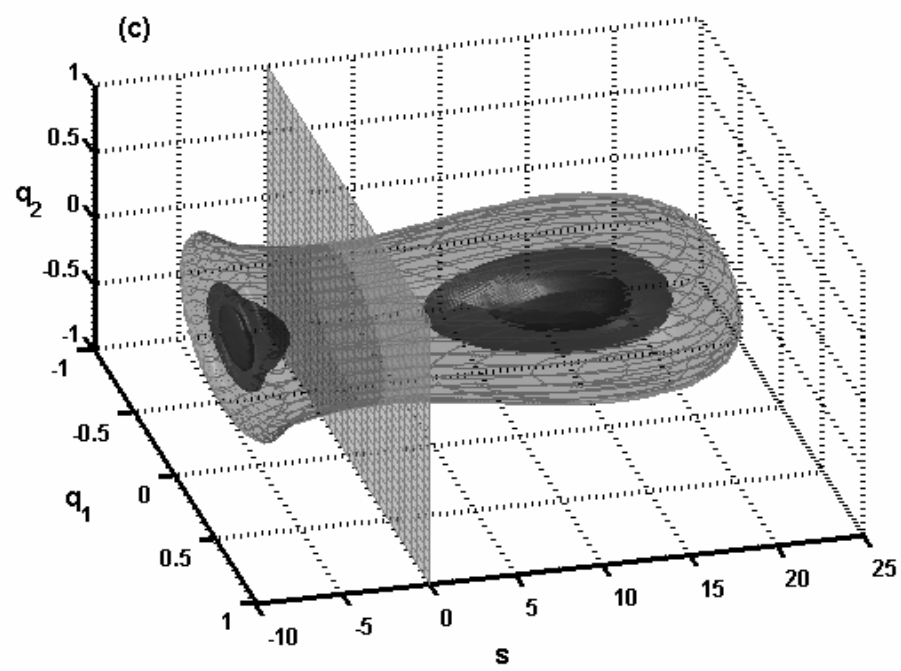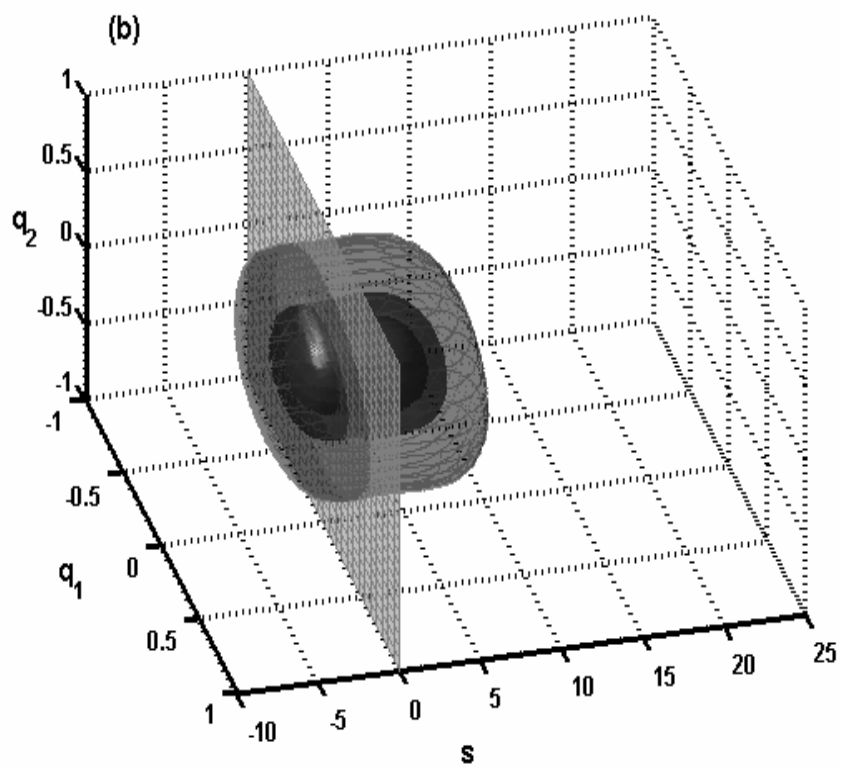
Chapter 5: The Generalized Moving Boundary Truncation Method

5.1 FAILURE OF THE DERIVATIVE PROPAGATION METHOD

Using DPM to propagate the boundary trajectories in MBT has been shown to be successful for model potential surfaces. Unfortunately, DPM is not applicable to all potential energy surfaces. For example, an attempt was made to propagate boundary trajectories on the collinear $H+H_2$ LEPS surface by Sato[31]. The trajectories are initially placed at the points where the density of a wave packet centered at [6.2, 1.4] has decayed to a value of 10^{-4}. In less than 1 f.s. of propagation, the DPM trajectories begin to cross and do not follow the contours of the potential surface or the motion of the wave packet being propagated on the fixed grid as shown in Figure 5.1. This leads to the question: why use trajectories at all?

If trajectories are not used, then some method must be used to adapt the boundaries in time. A natural choice is to activate grid points when the density is above a threshold and deactivate grid points when the density decreases below a threshold. In fact this approach has been pursued independently developed by McCormack [30] and Hartke [31]. In these methods, localized basis sets are added or eliminated based on fixed density parameters [30,31] or time dependent density parameters relative to the current maximum density [30]. Unfortunately, there are two main drawbacks to only monitoring density. First, an algorithm must be in place to prevent interior points near nodes from being eliminated. Second, density is not necessarily conserved. McCormack showed in scattering calculations that the density parameter for grid point activation needed to be lower than 10^{-8} in order for the transmission probability not to decay exponential away from the correct value. In fact, total density also decays exponentially.
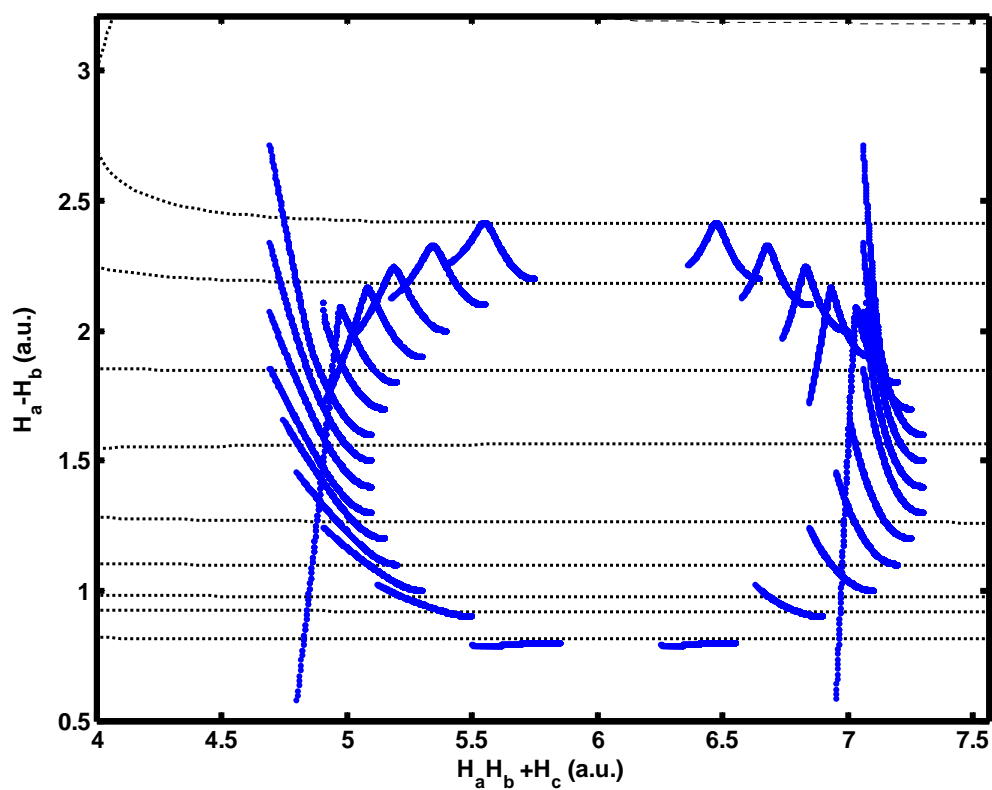
FIGURE 5.1 TRAJECTORY PATHS ON THE LEPS H+H_2 SURFACE AFTER 1.21 F.S. OF TIME PROPAGATION. The dotted lines represent contours of the potential surface. The blue lines are trajectories propagated with DPM, whose initial position was at density values of 10^{-4}.
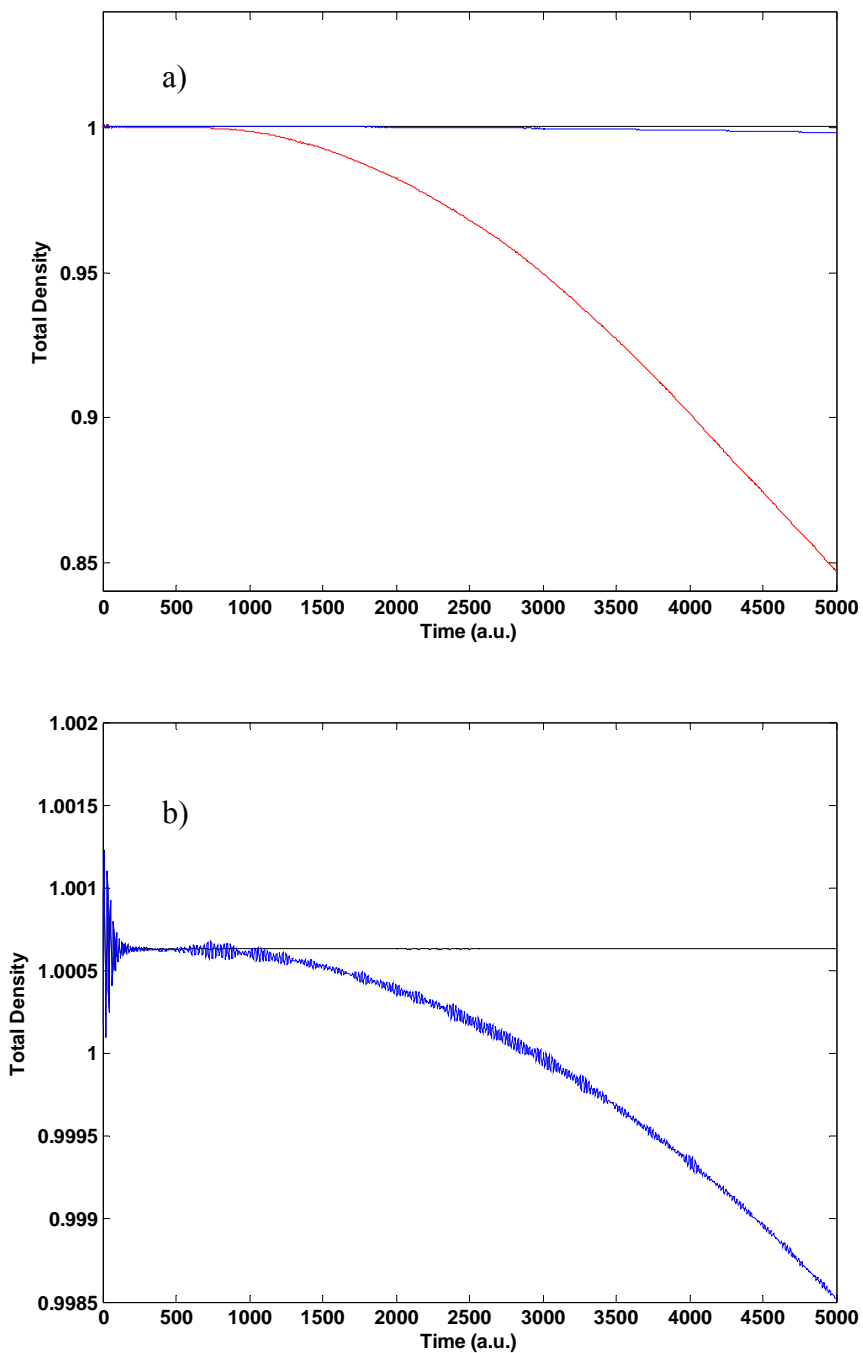
FIGURE 5.2 TOTAL DENSITY OF A WAVE PACKET SCATTERING ON THE H+H$_2$ LEPS SURFACE. The solid black line is the full fixed grid, the blue line has the density inclusion parameter set to 10^{-8} and the red line has the parameter set to 10^{-4}. a) Full view. b) zoomed view.

Figure 5.2 displays the total density of a wave packet scattering on the $H+H_2$ LEPS surface using fourth order finite differencing for spatial derivatives and a second order leap frog for the time propagator where the solid black line is the full fixed grid, the blue line has the density inclusion parameter set to 10^{-8} and the red line has the parameter set to 10^{-4}. From Figure 5.2a, it obvious that the latter is not a conservative method with respect to density. Setting the inclusion parameter to 10^{-8} appears to produce only minor errors. Close inspection in Figure 5.2b, however, shows the same exponential decay as in the 10^{-4} case with a different slope. If the calculation were continued for long times, using 10^{-8} as the density parameter would prove unsuccessful. Quantum trajectories are better at adapting the boundaries of a fixed grid because density is not necessarily conserved along a trajectory. In effect, the trajectories act as time adaptive density parameters. Since quantum trajectories do not cross, the portion of the wave packet contained in the trajectories (generally 99.99%) will always be contained within the trajectories. A new method for propagating the boundary trajectories has been developed in this work so that the MBT with quantum trajectories can be applied to an arbitrary potential energy surface.

5.2 THE MOVING BOUNDARY TRUNCATION METHOD ON ARBITRARY SURFACES

In order to apply the MBT to arbitrary surfaces, a propagation scheme similar to the QTM [11-14] is introduced for the trajectories. In QTM, a moving weighted least squares (MWLS) fitting procedure is used to determine ∇S and as such the Lagrangian velocity for the trajectories. In MBT, the trajectories may be too far apart to apply a MWLS fit using only the information carried by the trajectories. They are, however, always near underlying fixed grid points that carry the necessary information. Indeed, in MBT, the trajectories do not need to carry any information other than their position at each time step as all of the information needed to propagate both the wave packet and the

trajectories is embedded on the fixed grid. The new generalization of the MBT presented below exploits this advantage.

In order to calculate the velocity for a trajectory, the nearest fixed grid point is determined. Then all of the grid points within a predetermined distance will be included in a least-squares fit of S in a similar fashion to QTM. The main difference is that the fixed grid points carry the wave function in the Cartesian form, $A + iB$, rather than the polar form, $R\exp(iS)$, as is the case in QTM. The S function is calculated by taking $\tan^{-1}(B/A)$ at the fixed grid points that will be used in the moving weighted least squares (MWLS) fitting. This leads to the relative S, which may contain "saw tooth" features, due to the periodic nature of the $\tan^{-1}(B/A)$ function. Since only the gradient, ∇S, is needed for the trajectory velocity, a constant can arbitrarily be added to pieces of S without affecting the derivative. Specifically, each time the S function "jumps", $\pi/2$ is added or subtracted so that continuity is preserved. Detecting the jumps is straightforward at the edges of the wave packet since S is generally smooth. The smooth S that is generated differs from the absolute S only by a constant; the slope of S is preserved which is the only quantity of interest for calculating the gradient, ∇S. The MWLS fitting procedure is applied to the new smooth S as outlined in the QTM. The ∇S determined by MWLS is used to generate the Lagrangian velocity of the trajectories and the trajectories can then be propagated in time.

One issue that can occur using the previous scheme is spreading or compression of the trajectories. When spreading occurs, the edges of the grid may not be correctly chosen. When compression occurs, more trajectories than are necessary to determine the edges of the fixed grid are being propagated. As a solution, the trajectories are periodically checked to insure they are within a minimum and maximum distance of each

other. Trajectories can be discarded and created as desired because all the information needed for propagation is being carried by the fixed grid.

The first application of the generalized MBT is the collinear $H_A+H_BH_C$ reaction on the LEPS surface [31]. The wave function dynamics are solved in the Jacobian coordinate system where R is the distance between the incoming HA atom and the center of mass of the reactant diatomic and r is the separation of the diatomic. The initial wave packet is the product of a Gaussian wave packet in R and the ground state of a Morse oscillator in r:

$$\psi(R,r,t=0) = \sqrt{\frac{\alpha}{\pi}} \exp\left[-\frac{\alpha}{2}(R-R_0)^2 - ip(R-R_0)\right]\phi_0(r) \tag{5.1}$$

The initial parameters for the wave packet are $\alpha = 8.0$, $R_0 = 4.5$, $p = [-4.875, -0.375]$ and ϕ_0 represents the ground state of the H_2 Morse oscillator centered at $r = 1.40083\, a.u.$. The wave function is propagated on a fixed grid with spacing $\Delta R = \Delta r = 0.05\, a.u.$ and the trajectories are started at points where density of the initial wave packet has decayed to 10^{-4}. The numerical methods used to propagate the wave function are similar to earlier examples: fourth-order finite differencing is used to calculate the kinetic energy operator and a second order leap frog method is used to advance the wave function in time with a time step of $\Delta t = 0.25\, a.u.$. The transmission region for this example is all $[R,r]$ where the distance from H_A to H_B is less than the distance from H_B to H_C. The transmission probability is calculated by:
$$P_{trans} = \iint_{H_AH_B<H_BH_C} \psi^*\psi\, dRdr.$$

Wave packets with various initial kinetic energies were propagated for 90.75 fs and the results are summarized in Figure 5.3. The transmission probabilities of the MBT
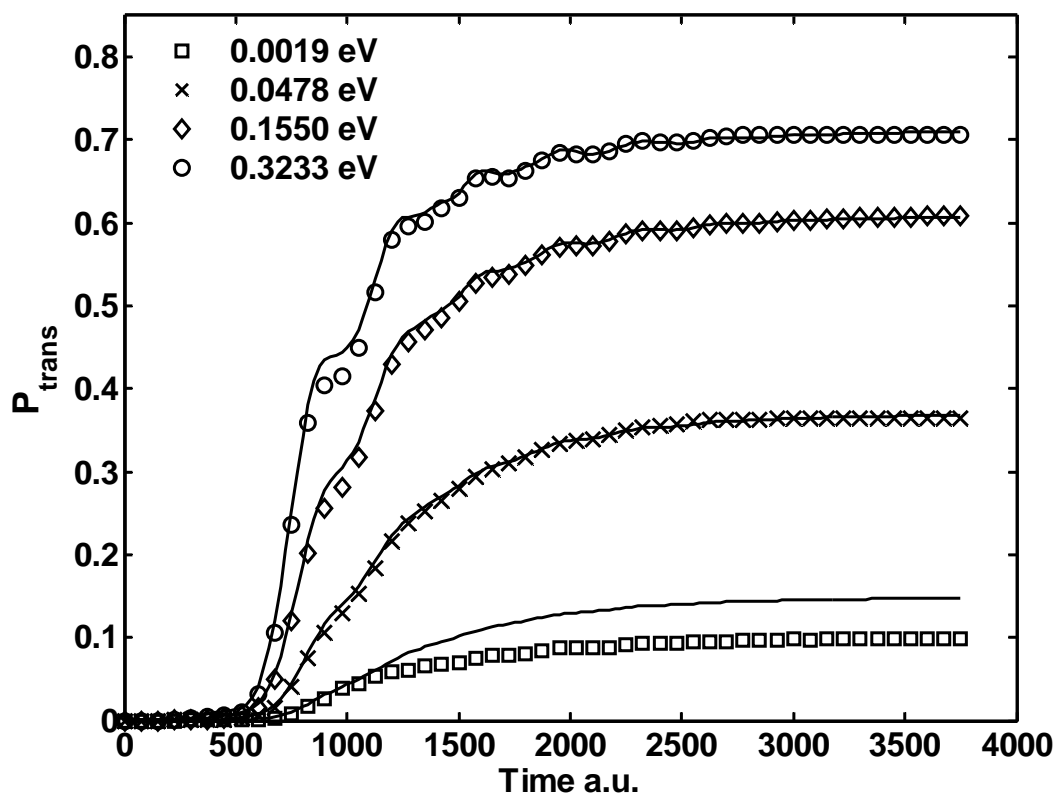
FIGURE 5.3. TRANSMISSION PROBABILITIES FOR THE COLLINEAR $H+H_2$ REACTIONS FOR VARIOUS INITIAL KINETIC ENERGIES. The Markers indicate the MBT calculation while solid lines indicate the full grid solutions. The difference in results can be reduced by moving the initial trajectory positions further from the center of the initial wave packet.

propagation are compared to those using grid whose boundaries are fixed at the minimum and maximum values achieved in each degree of freedom, $[R, r]$, by the MBT solution. The two methods are in excellent agreement. The MBT produces transmission probabilities that differ by only 1.13% for the top three initial kinetic energies. The MBT results for the lowest kinetic energy (0.0019 eV) differ by 32%. If the trajectories are started at density values of 10^{-6} rather than 10^{-4}, the error difference is reduced to 10.21% and if the initial trajectories are moved to density values of 10^{-8}, the error is reduced even further to 1.59%. Not only is the MBT extremely accurate in the converged transmission probability, but it captures the resonance patterns in transmission probabilities as seen in the 0.3233 eV and 0.1550 eV calculations.

While maintaining accuracy, the MBT is much more efficient than the full grid calculations. The full grid averaged 121 minutes and uses 1,074,316 grid points at each time step. The MBT calculations averaged only 15 minutes on the same computer; an 87.6% reduction in computational time. The reason for the MBT efficiency is shown in Figure 5.4. Although extra resources are necessary to propagate the trajectories, only 60 trajectories are needed initially as H_A approaches the diatomic (Fig. 5.4a) moving towards $R = 0$ while the wave packet remains essentially a Gaussian in r. The 60 trajectories determine the boundaries of a fixed grid containing only 1514 grid points. A more detailed view of the initial wave packet is displayed in Figure 5.4b. This figure shows how the trajectories are initially started at equally spaced points corresponding to fixed grid points. Some of the trajectories are close together while others, particularly at the edges of r are farther apart. Immediately after propagation begins, the algorithm will adaptively eliminate trajectories that are too close ($<0.07 a.u.$) or add trajectories if the distance between existing trajectories is too large ($>0.5 a.u.$). As the wave packet spreads into the product channel, more trajectories are added (Fig. 5.4c) increasing the number to

FIGURE 5.4. CONTOURS OF THE MBT H+H$_2$ COLLINEAR REACTION CALCULATION FOR A WAVE PACKET WITH AN INITIAL KINETIC ENERGY OF 0.3233 EV. Filled contours represent the wave packet density ranging from 0.0001 in dark blue to 0.1 in red. Green points represent trajectory locations. Dashed contours represent the LEPS potential energy surface. Solid red lines indicate the boundary of the fixed grid used to propagate the wave packet. (a) Initial wave packet with 60 trajectories set at the edges of the 0.0001 contour. (b) Close up oh the initial wave packet and trajectories. (c) Wave packet after 45 fs of propagation. The trajectories have spread and their number has increased to 234 in order to correctly cover the points needed to advance the calculation. (d) Final wave packet after transmission probability has converged. The number of trajectories has increased to 512.

t=45 f.s. (c)

t=90.75 f.s. (d)
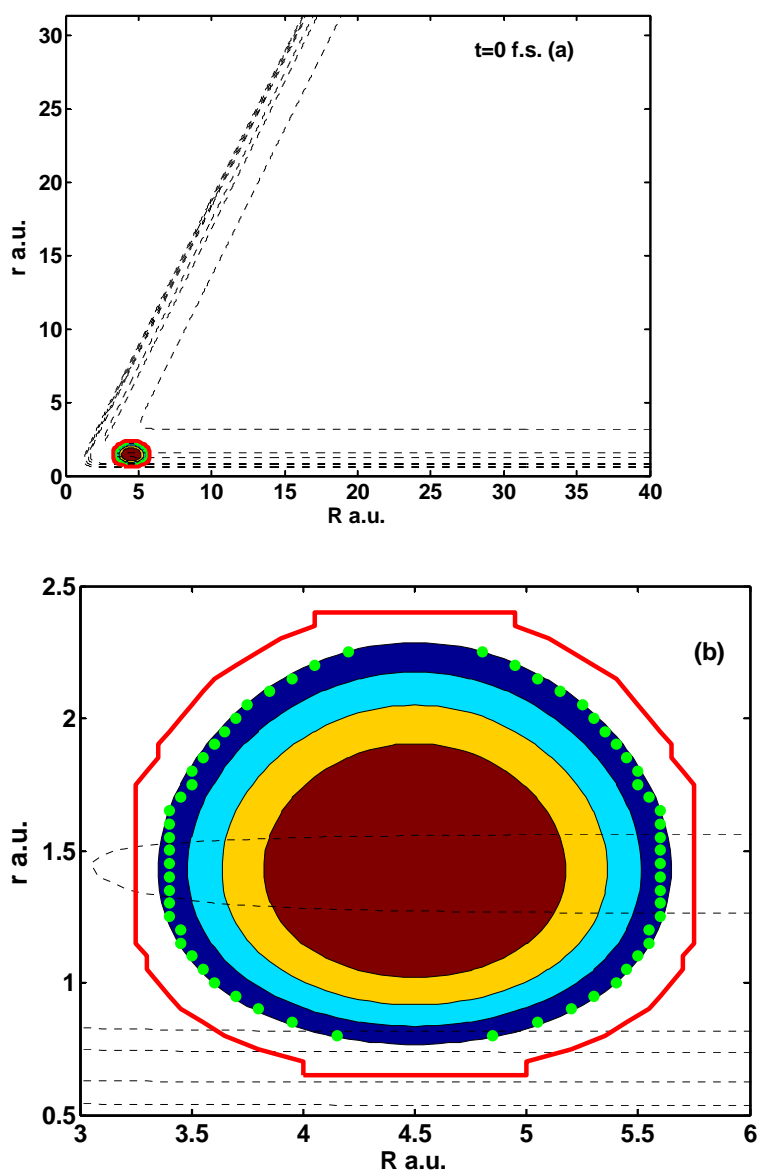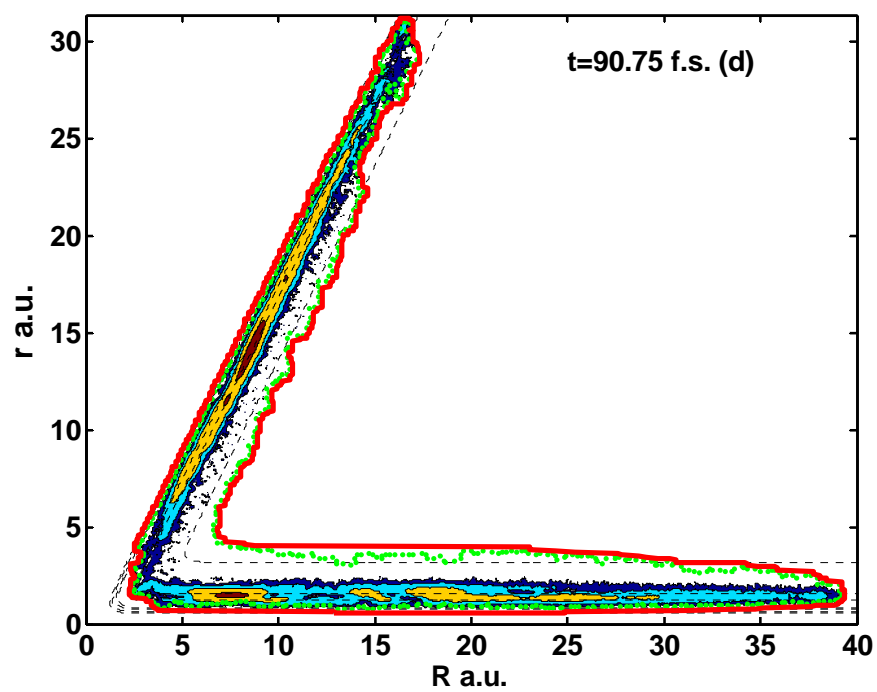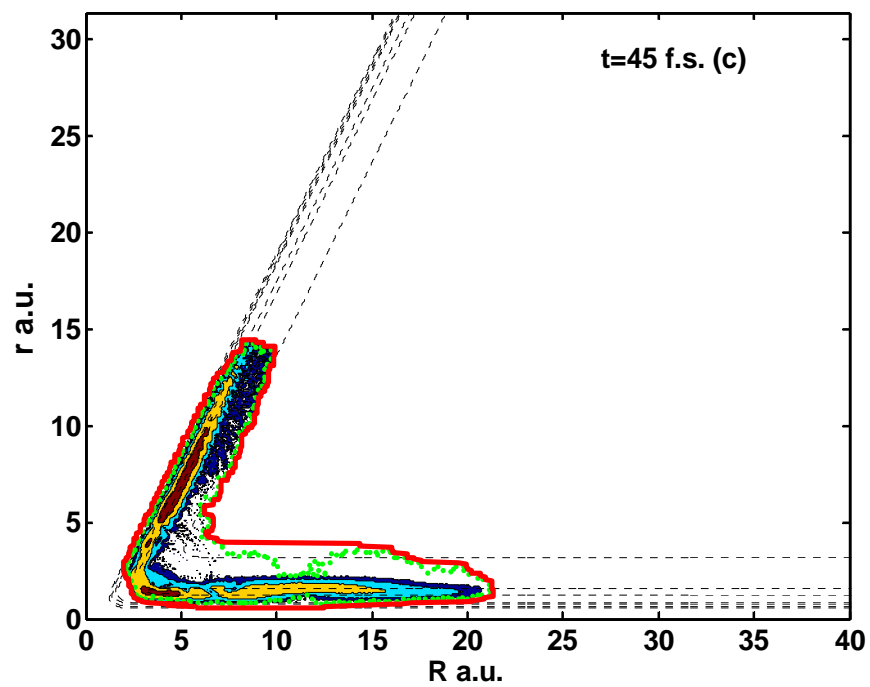
234. The boundaries of the fixed grid are adapted according to the motion of the trajectories, increasing the grid size to 34,906 points halfway through the propagation. Once the transmission probability is converged (Fig. 5.4d) and the propagation is complete, the wave packet has nearly bifurcated. The calculation finishes with 512 trajectories and 76,382 fixed grid points. The increase in the number of trajectories and grid points is nearly linear throughout the propagation of the wave packet. The trajectories define the reactant and product channel with no advance information about the potential energy surface. This means that no unnecessary grid points in the dissociative region are added into the calculations. Also, by calculating the wave function in the Jacobi frame, interference effects are resolved without numerical difficulties. If further propagation were desired, the trajectories could be used to create two separate wave packets as described in the previous chapter.

5.3 OTHER NUMERICAL PROPAGATORS AND THE MOVING BOUNDARY TRUNCATION METHOD

The next example extends the MBT method to other numerical methods besides finite differences. Specifically, a nonrotating atom+diatomic reactive system in three Jacobi coordinates $\{R, r, \theta\}$ is solved, where once again R is the distance between the incoming atom and the center of mass of the reactant diatomic, r is the reactant diatomic bond length, and θ is the angle between R and r. The total angular momentum is set to zero and the motion of the center of mass is eliminated so that the Hamiltonian becomes:

$$\hat{H} = -\frac{1}{2M}\frac{\partial^2}{\partial R^2} - \frac{1}{2m}\frac{\partial^2}{\partial r^2} - \frac{1}{2\mu}\left(\frac{\partial^2}{\partial\theta^2} + \cot\theta\frac{\partial}{\partial\theta}\right) + \hat{V}$$

(5.2a)

or

$$\hat{H} = \hat{T}(R,r) + \hat{J}(\theta) + \hat{V}(R,r,\theta)$$

where

$$\hat{T}(R,r) = -\frac{1}{2M}\frac{\partial^2}{\partial R^2} - \frac{1}{2m}\frac{\partial^2}{\partial r^2}$$

$$\hat{J}(\theta) = -\frac{1}{2\mu}\left(\frac{\partial^2}{\partial \theta^2} + \cot\theta\frac{\partial}{\partial \theta}\right)$$

(5.2b)

with the moment of inertia: $\dfrac{1}{\mu} = \dfrac{1}{MR^2} + \dfrac{1}{mr^2}$.

The specific reactive system is $O(^3P) + H_2(v=0; j=0) \rightarrow OH + H$ on the $^3A'$ potential energy surface presented earlier. The initial wave packet used for all calculations is a product of Gaussians in $\{R,r\}$:

$$\psi(R,r,t=0) = \sqrt{N}\exp\left[-\alpha(R-R_0)^2 - \beta(r-r_0)^2 - ip(R-R_0)\right]$$

(5.3)

With initial values of $\alpha = 4.0, \beta = 9.06, R_0 = 6.0, r_0 = 1.444, p = [-18,-6]$.

In order to efficiently propagate the wave packet, the split operator method is applied to the Hamiltonian as follows:

$$\psi_{t+\Delta t} = \exp(\frac{-i\Delta t}{2}\hat{J}) * \exp(\frac{-i\Delta t}{2}\hat{V}) * \exp(-i\Delta t\hat{T}) * \exp(\frac{-i\Delta t}{2}\hat{V}) * \exp(\frac{-i\Delta t}{2}\hat{J})\psi_t$$

(5.4)

A fast Fourier transform (FFT) is used to calculate the kinetic energy operator $\hat{T}(R,r)$ and the discrete variable representation (DVR) is used for the rotational operator $\hat{J}(\theta)$. The grid for the FFT calculations is 256x256 with grid spacing $\Delta R = \Delta r = 0.08$ Sixty divisions of θ were used in the DVR calculations. Complete explanations of these two methods are widely available in literature, but summaries are provided here to emphasize how MBT can enhance their performance. The FFT transforms position space, $[R,r]$, to momentum space, $[P,p]$, thus simplifying the derivative operator to a multiplication. The transform is accomplished numerically by changing the integral to a discrete sum:

$$\psi_{j,k}(P,p) = \sum_{l=0}^{N_R-1}\sum_{m=0}^{N_r-1}\psi_{l,m}(R,r)\exp(\frac{-2\pi i}{N_R N_r}lm)$$

(5.5)

In Equation 5.5, $\psi_{j,k}(P,p)$ is the representation of the wave function in momentum space at point $[P_j, p_k]$. It is the weighted sum of the representation of the wave function in position space, $\psi_{l,m}(R,r), l=1,...N_R, m=1,...N_r$, where N_R and N_r are the total number of points used in position space. At first glance, this would seem to be an ideal candidate for MBT, as the sum could be limited to only points within the boundary defined by the trajectories. As numerical algorithms for Fourier transforms have been developed over the years, however, symmetry properties of the transform have been exploited to reduce the overall number of terms that are actually calculated. For all of the available algorithms for FFT, the vector lengths in position space and momentum space must remain equal. This means that when MBT is applied to an FFT, either the number of points in momentum space is reduced to match the number of points in the truncated grid, or the truncated grid can be padded with zeroes in order to maintain the appropriate number of momentum points required for a stable propagation. In the former case, the propagation quickly becomes unstable and inaccurate because the spacing in momentum is either too large or the minimum and maximum of the momentum space is limited. In the latter case, there is no efficiency gained by placing zeroes around the truncated grid. If an FFT algorithm was developed that could maintain the speed of symmetry based methods while allow vectors of different lengths in position and momentum spaces, then MBT may be applicable to an FFT propagation.

The ideal application of MBT is in the rotational operator. The discrete variable representation (DVR) takes the wave function represented by a point basis and transforms it to a function basis. The reason that the DVR is preferred over an FFT for the rotational operator is the $\cot\theta\dfrac{\partial}{\partial\theta}$ term. Unlike the second derivative term in the kinetic energy operator, this term does not translate to a simple multiplication in momentum space. In DVR, a unique transformation matrix, Y, is used to transform the wave function from a

number of points in θ to a basis set, usually that of a harmonic oscillator. In addition to being able to transform the wave function, any operator can also be transformed, $\hat{A}_{DVR} = Y \hat{A}_{HO} Y^{+}$. In this application of DVR only points along θ are required and the transform is independent of $\{R,r\}$. When MBT is applied to the mixed FFT-DVR calculation, trajectories move along $\{R,r\}$ in discrete divisions of theta that will be used as DVR points. The minimum and maximum locations of the trajectories define a box in $\{R,r\}$. Only the points inside the box are used as DVR points in the transformation and thus only these points have the rotational operator applied to them. Initially, there are 2,760 trajectories divided evenly among the 60 θ divisions and placed in $\{R,r\}$ where the density of the wave packet has decayed to 10^{-4} (Figure 5.5a). This creates a box of 73,800 grid points in which the rotational operator is applied. As the trajectories move, the box of grid points moves with them, selectively applying the rotational operator only to the points where the density of the wave packet is significant. The number of trajectories and grid points used in the DVR stays relatively constant until the wave packet enters the transition state at approximately 21 fs (Figure 5.5b). At this time, the trajectories have properly adapted the boundaries of the grid used in the DVR calculation so that the rotational operator is applied to produce the correct dynamics. After the wave packet has begun to enter the product tubes, both the number of trajectories and the number of grid points in the DVR calculation increase linearly until their final values, 6,544 and 697,080 respectively, at the end of the propagation.

The advantages of MBT are visualized in Figure 5.5. In this figure, the axis are cylindrical in that R lies along the x axis, r is the absolute distance from the x axis, and positive θ is counter-clockwise rotation around the x axis. Examination of the potential isosurface $V = 0.75$ eV, best seen in Figure 2.3c in Chapter 2, shows that the rotational operator is not critical in the initial stages as the potential is evenly distributed around θ

in a tube shape. In the transition region at approximately $R = 3a.u.$, rotation is critical as the potential develops minima near $\theta = 0$ and $\theta = \pi$. The product tubes then quickly redistribute to encompass the entire range of θ. If rotation is neglected from the Hamiltonian, this important feature of the potential energy surface would be lost and calculated values for the transmission probability are significantly lower than the correct values. With MBT, the rotational effects are preserved, but limited to the points inside the boundaries defined by the trajectories. As the packet enters the transition state region (Fig. 5.5b), the effect of the rotational operator allows the packet to correctly spread through the $\theta = 0$ and $\theta = \pi$ regions. The trajectories continue to guide the MBT grid down the two product tubes until the transmission probability is full converged, shown in Figure 4c. Comparing Figures 4c and 4d, reveals that the wave packet on the MBT grid has a small amount of numerical artifacts on the leading edges of the transmitted portions that are not present in the full grid wave packet. This difference in the wave packets is only evident after transmission probability has converged and does not appear to affect the stability or accuracy of the MBT calculation.

The performance of MBT is displayed in Figure 5.6. The transmission probability of both the MBT and the full fixed grid are nearly in exact agreement for the O(^{3}P) +H$_2$($v = 0; j = 0$) reaction (Fig 5.6a). The error ranges from 0.15% to 2.03% with the largest error being at the lowest kinetic energy. Figures 5.6b and 5.6c show the two transmission probabilities for the O(^{3}P) +HD($v = 0; j = 0$) reaction. The dramatic influence of the rotational operator is demonstrated here by the large difference in transmission probability between the OH and OD products. Once again the MBT is just as accurate as the full grid calculation with a maximum difference in OH transmission probability of 0.49% and OD transmission probability of 8.99% and capturing resonance patterns as transmission probability develops over time. The maximum errors are at the

lowest energies. The OD transmission probability at the lowest initial energy is only 0.0128. The error at higher energies drops to 1% or less. The reason for the increased error at the lowest kinetic energy is that the trajectories have eliminated the low density edges ($<10^{-4}$) of the wave packet. These low density edges are responsible for tunneling effects. In a similar fashion to the collinear H+H$_2$, the initial trajectories could be extended outward to capture more of the initial wave packet and thus capture more of the tunneling. These excellent results are obtained much more efficiently than the full grid calculations. An average full grid calculation takes an average of 212 minutes. The MBT only takes 75 minutes, a reduction of 65%.

FIGURE 5.5. WAVE PACKET PROPAGATION OF THE $O(^3P) + H_2(v = 0; j = 0) \rightarrow OH + H$ REACTION ON THE $^3A'$ POTENTIAL ENERGY SURFACE. Red isosurfaces indicate the potential energy surface at $V = 0.75eV$. Isosurfaces of the wave packet a t a density of 0.0001 are colored blue. (a) Initial wave packet. The points used in the rotational operator are only contained in the blue wave packet isosurface. The potential surface breaks into two tubes along $\theta = 0$ and $\theta = \pi$ at approximately $R = 2.5a.u.$. (b) Wave packet after 21.78 fs. The MBT has guided the wave packet correctly into the two product tubes. (c) Wave packet after transmission probability has converged (60.5 fs). The wave packet has fractured into three distinct parts and MBT restricts the rotational operator to only these areas. The leading edge of the transmitted packets shows some numerical artifacts not present in the full grid. (d) Full grid wave packet after 60.5 fs.
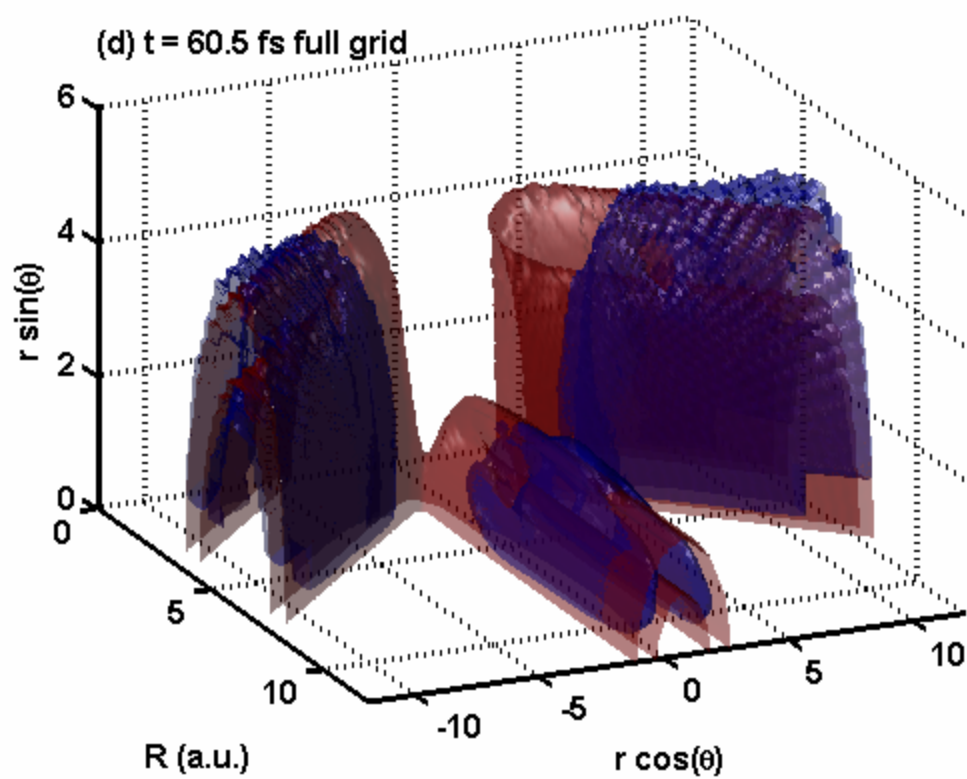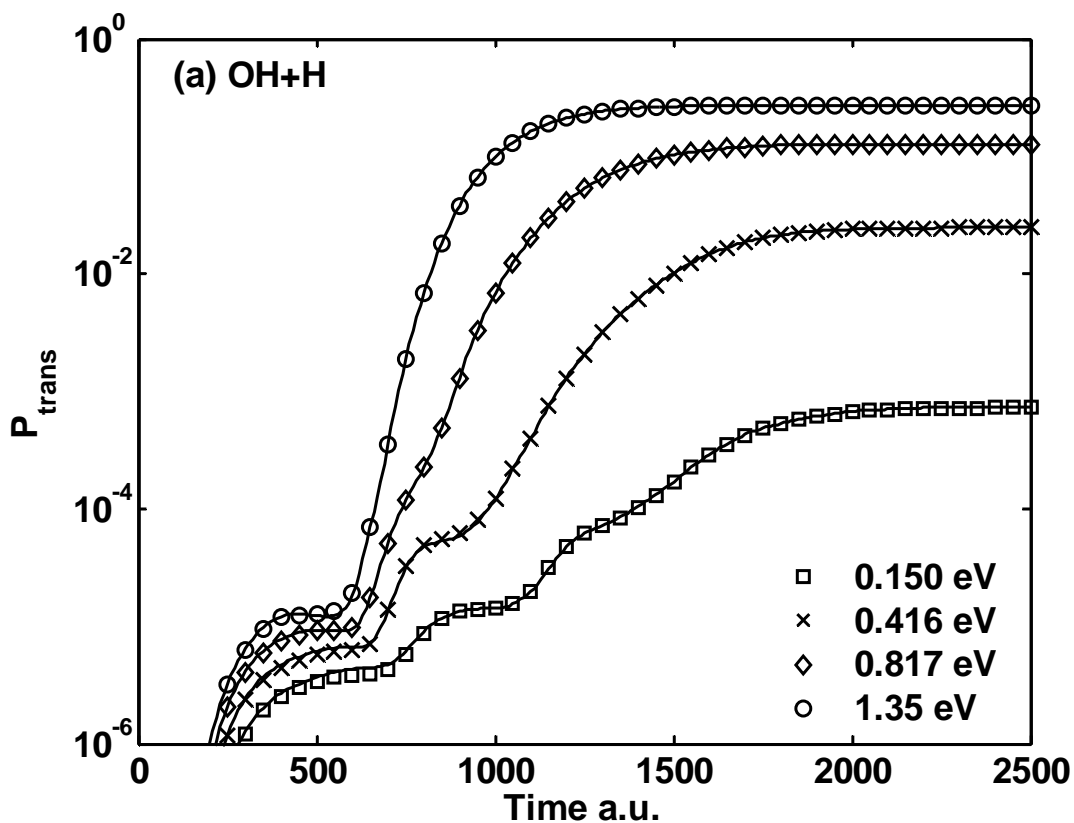

-65-

(b) t = 21.78 fs MBT grid

(c) t = 60.5 fs MBT grid

(d) t = 60.5 fs full grid
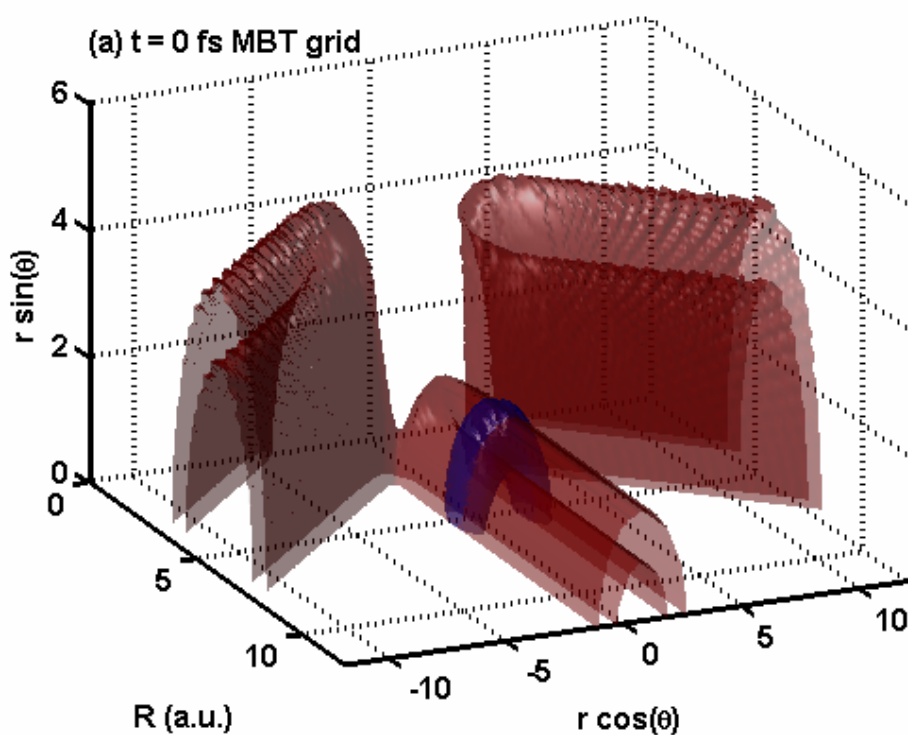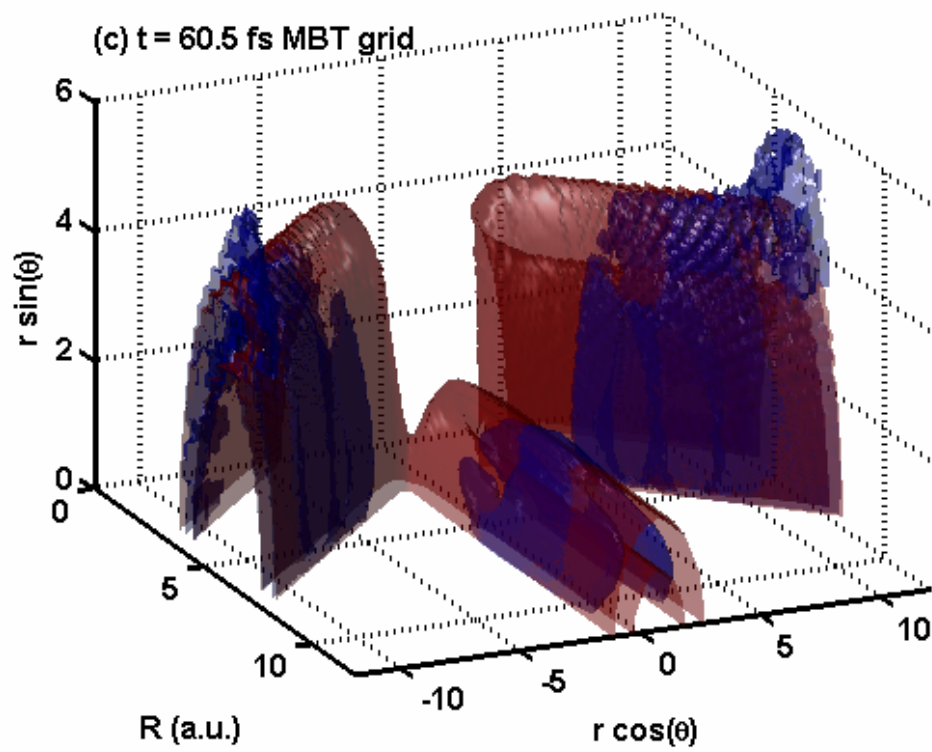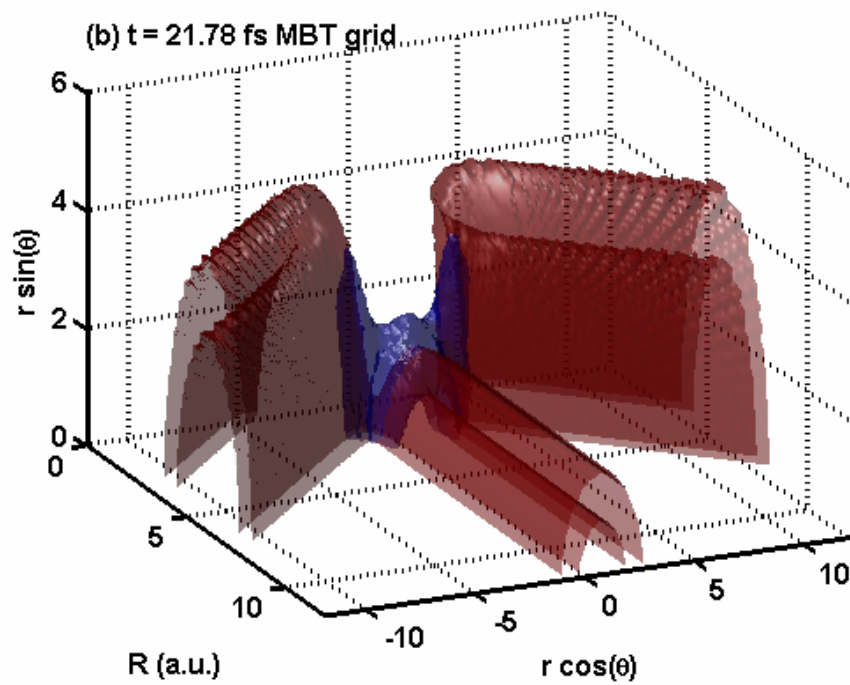
FIGURE 5.6. (A) TRANSMISSION PROBABILITIES FOR THE O(^{3}P) +H$_2$($v = 0; j = 0$)
REACTION FOR VARIOUS INITIAL KINETIC ENERGIES. The markers indicate the MBT
calculation while solid lines indicate the full grid solutions. Transmission probability (y
axis) is on a logarithmic scale for clarity. (b) The OH transmission probabilities of the
O(^{3}P) +HD($v = 0; j = 0$). (c) The OD transmission probabilities of the O(^{3}P)
+HD($v = 0; j = 0$).

(b) OH+D

- □ 0.150 eV
- × 0.416 eV
- ◇ 0.817 eV
- ○ 1.35 eV

(c) OD+H

0.150 eV
0.416 eV
0.817 eV
1.35 eV
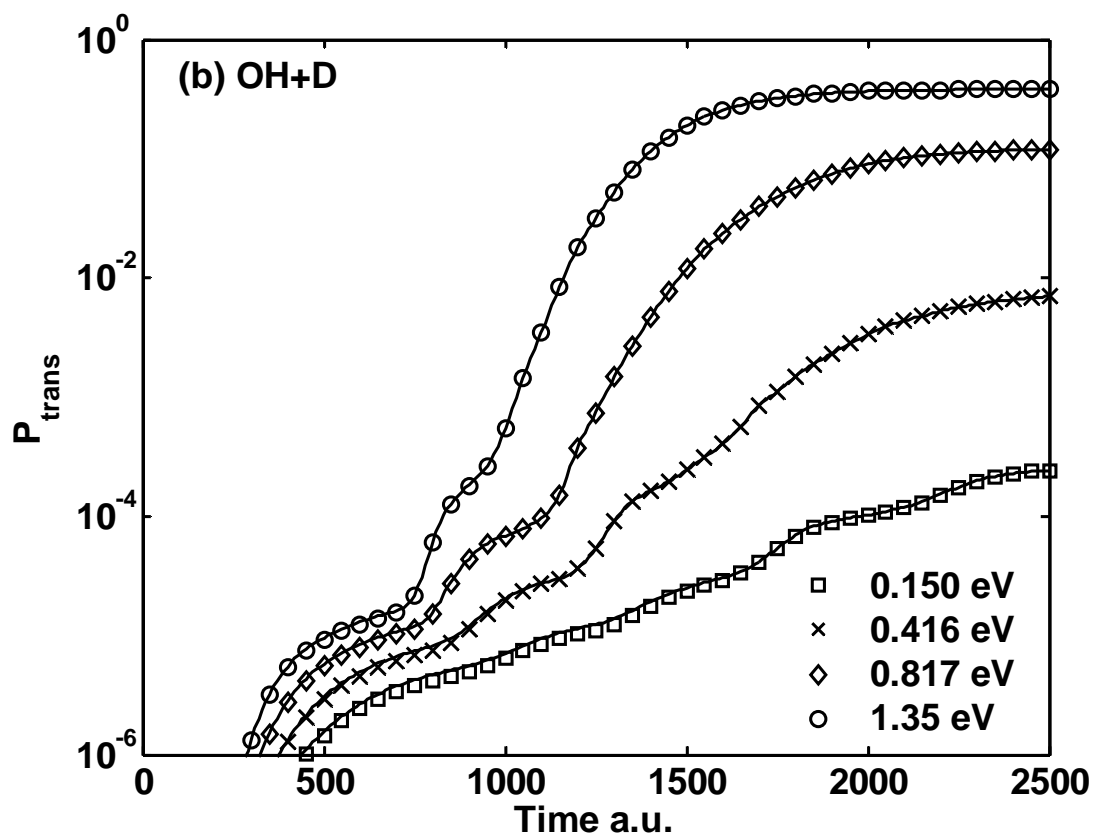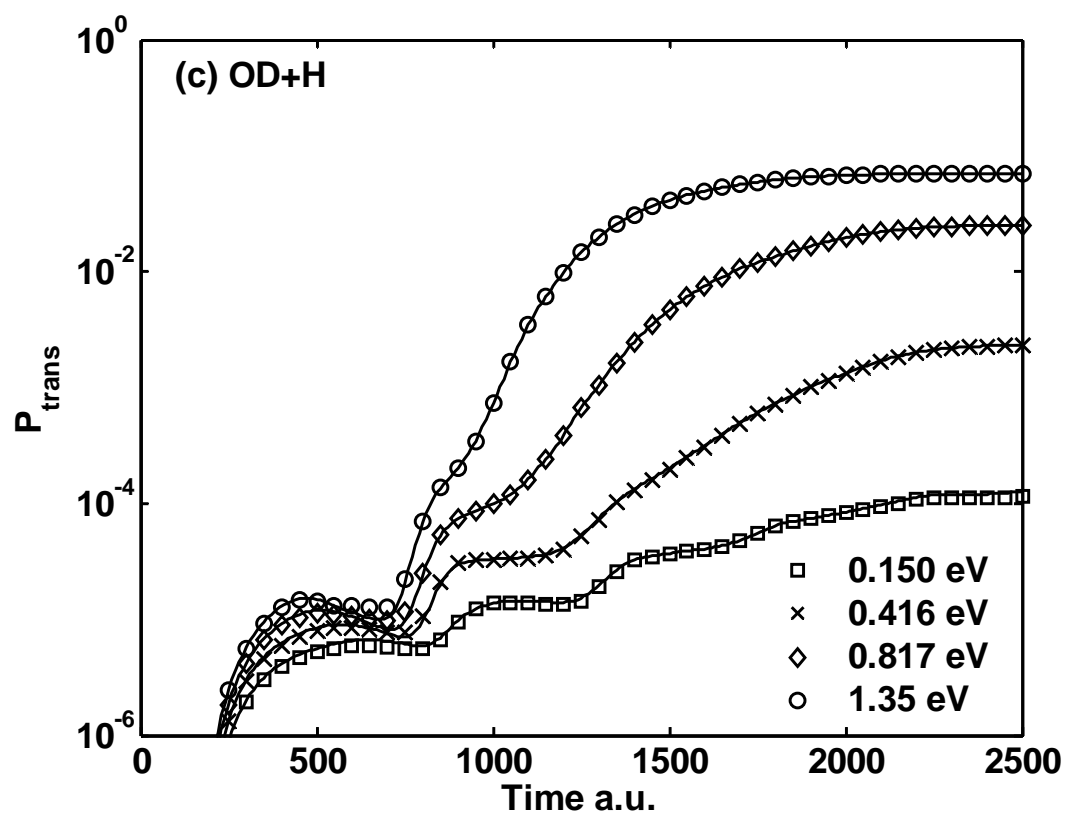
Chapter 6: Conclusion

In this work, a new method for numerically integrating the time dependent Schrödinger equation was presented. The moving boundary truncation (MBT) method works on the principle that during a quantum transport calculation, only certain grid points are important to the dynamics of the system. The boundaries of the grid are moved according to the positions of quantum trajectories whose motion is governed by the quantum hydrodynamic equations of motion (QHEM). The various methods for numerically integrating of these equations were the inspiration for this work. The details of their implementation and their advantages and disadvantages were discussed.

The initial formulation of the method relied on using the derivative propagation method (DPM) for moving the boundary trajectories. DPM was chosen because this method allows trajectories to be propagated independently of each other and eliminates any errors from spatial fitting. The method was successful when using DPM to propagate the boundary trajectories on a variety of model potential energy surfaces and up to three degrees of freedom. Unfortunately, DPM is not a stable propagator for all potential energy surfaces so a generalized variation of MBT was required.

The generalized method relies on reconstructing a relative quantum action function S from the Cartesian wave function through $\tan^{-1}(B/A)$ and smoothing the periodic nature of the inverse tangent function. After smoothing, a moving weighted least squares (MWLS) fit is applied to determine ∇S and move the trajectories. This new variation was first successfully applied to the H+H$_2$ collinear reaction (using a LEPS potential surface) finite differencing used to determine spatial derivatives. The MBT was then extended to more complex surfaces and numerical methods by calculating the O(^{3}P) +H$_2$($v = 0; j = 0$) $\rightarrow$ OH +H reaction on the $^3A'$ potential energy surface. This example

showed that MBT can be selectively applied to certain degrees of freedom in a multi-dimensional calculation using any grid based numerical method. This could prove useful in problems with a large number of degrees of freedom where certain degrees of freedom are calculated in total and others are truncated. The MBT method is not only efficient, but very accurate. The highest errors are always in low energy calculations. To increase accuracy for these situations, the initial trajectories can be set further from the center of the wave packet.

The moving boundary truncation method presented in this work is a robust numerical method for integrating the time dependent Schrödinger equation. The method is nearly as accurate as methods that use many more grid points. A variety of numerical methods for generating spatial derivatives were demonstrated to be compatible with MBT. The method was also applicable to a variety of potential energy surfaces not previously solved by traditional trajectory methods such as QTM, DPM, or ALE. The MBT method is an efficient, accurate choice for calculating chemical quantum dynamics.

Although the advantages of MBT have clearly been presented in this work, the disadvantages have not been fully explored. A difference, although small, in transmission probability was observed between the MBT grids and full grids. Future developments in the method could study correlation between the initial placement of trajectories and the difference in transmission probability between the MBT and full grid. If this could be related to initial wave packet energy, barrier height, or a combination of the two, then a selection criteria could be developed based on desired accuracy.

Another difference between the MBT calculations and full grid calculations were the oscillations in density near the edges of the wave packet. This is probably a purely numerical artifact since all numerical methods can develop errors if the boundaries are not carefully chosen. This should be studied in detail, however, to insure that there are no

stability issues associated with the oscillations. Multiple barrier surfaces would provide excellent insight into this issue.

Aside from deeper examination of the method itself, there are two other main areas of future research concerning the MBT method. The first would be a continuation of this work by applying MBT to various numerical propagators. Each numerical technique has unique issues with boundary conditions. Some, such as the FFT discussed in Chapter 5, are not well suited to boundary truncation. Others, such as the Chebyshev pseudospectral techniques used by Hughes and Wyatt [23], rely on fixed grid points and may benefit from having the boundaries truncated. A natural first step in this direction would be to use quantum trajectories in the methods developed by McCormack [34] and Hartke [35]. These methods rely on a density parameter for boundary truncation and thus suffer from accuracy and conservation issues as discussed earlier. If quantum trajectories were used at the boundaries as in MBT, the conservation of density should be insured and the accuracy should increase.

A second direction of future research would be expanding the application of MBT. There are a variety of quantum mechanical problems that may benefit from MBT. A typical example not yet studied would be a reaction in which two electronic states are close in energy. In these problems, transitions can occur between the two electronic states. The MBT method could be used to keep the higher energy electronic state completely deactivated until the trajectories reach areas of the lower energy state where crossing can occur. The MBT could also be extended to other partial differential equations besides the Schrödinger equations. There are a variety of transport equations which may benefit from adaptive boundaries such as those in the moving boundary truncation method.

Bibliography

1. I. Vorobeichik, N. Moiseyev, J. Phys. B **31,** 645 (1998).

2. H. Masui and Y. K. Ho, Phys. Rev. C **65,** 054305 (2002).

3. O. Shemer, D. Brisker, N. Moiseyev, Phys. Rev. A **71**, 032716 (2005).

4. R. E. Wyatt, Quantum Dynamics with Trajectories, Springer, New York, 2005.

5. C. L. Lopreore, R. E. Wyatt, Phys. Rev. Lett. **82,** 5191 (1999).

6. R. E. Wyatt, Chem. Phys. Lett. **313**, 189 (1999).

7. R. E. Wyatt, J. Chem. Phys. **111**, 4406 (1999).

8. R. E. Wyatt, E. R. Bittner, J. Chem. Phys. **113**, 8898 (2000).

9. J. B. Maddox, E. R. Bittner J. Chem. Phys. **119**, 6465 (2003).

10. D. Bohm, Phys. Rev. **85**, 166 (1952).

11. D. Bohm, Phys. Rev. **85**, 180 (1952).

12. C. J. Trahan, K. Hughes, R. E. Wyatt, J. Chem. Phys. **118**, 9911 (2003).

13. C. J. Trahan, R. E. Wyatt, B. Poirier, J. Chem. Phys. **122**, 164104 (2005).

14. S. Garashchuk and V. A. Rassolov, Chem. Phys. Lett. **376**, 358 (2003).

15. S. Garashchuk and V. A. Rassolov, J. Chem. Phys. **120,** 1181 (2004).

16. V. A. Rassolov and S. Garashchuk, J. Chem. Phys. **120,** 6815 (2004).

17. D. Babyuk, R. E. Wyatt, J. Chem. Phys. **121,** 9230 (2004).

18. D. Babyuk, R. E. Wyatt, Chem. Phys. Lett. **400,** 145 (2004).

19. B. K. Kendrick, J. Chem. Phys. **119,** 5805 (2003).

20. D. K. Pauler, B. K. Kendrick, J. Chem. Phys. **120,** 603 (2004).

21. B. K. Kendrick, J. Chem. Phys. **121,** 2471 (2004).

22. C. J. Trahan, R. E. Wyatt, J. Chem. Phys. **118,** 4784 (2003).

23. K. H. Hughes and R. E. Wyatt, Chem. Phys. Lett. **366,** 336 (2002).

24. D. Babyuk and R. E. Wyatt, Chem. Phys. Lett. **387,** 227 (2004).

25. M. J. Baines, Moving Finite Elements, Oxford Science Publications, New York, 1994.

26. S. Li, L. Petzold, Y. Ren, SIAM J. Sci. Comput. **20,** 719 (1998).

27. L. Pettey, R.E. Wyatt, Chem. Phys. Lett. **4-6**, 424 (2006).

28. L. Pettey, R.E. Wyatt, Int. J Quant Chem. **107**, 1566 (2007).

29. L. Pettey, R.E. Wyatt, J. Chem Phys. Accepted for publication 10/2008.

30. C. Eckart, Phys. Rev. **35**, 1303 (1930).

31. S. Sato, J. Chem. Phys. **23**, 592 (1954).

32. S. Rogers, D. Wang, A. Kuppermann, S. Walch, J. Phys. Chem. A **104**, 2308 (2000).

33. C.J. Trahan, R.E. Wyatt, J. Comp. Phys. **185,** 27 (2003).

34. D. McCormack, J. Chem. Phys. **124**, 204101 (2006).

35. B. Hartke, Phys. Chem. Chem. Phys. **8**, 3627 (2006).

Vita

Lucas Richard Pettey was born November 12,1974 in Johnson City, New York. He is the son of Frank Paul Pettey and Karen Winner Pettey both retired public school teachers. He has one older brother, Christopher Joseph Pettey. After graduating from high school at Lincoln Park Academy in 1993, he entered the University of Central Florida in pursuit of a Bachelor of Science in Chemistry. Upon graduation in 1998, Lucas decided to remain at UCF in order to obtain his Master of Science in Industrial Chemistry. He developed and studied a new method for removing NO_x emissions from flue gases as his thesis which resulted in three publications. He entered graduate school at the University of Texas at Austin in the Fall of 2002. Since then, he has worked under the supervision of Robert E. Wyatt and produced three publications concerning a new method for integrating the time dependent Schrödinger equation.

Permanent address: 15424 Fernhill Drive Austin, Texas 78717.

This dissertation was typed by the author.